SANDIA REPORT
SAND2012-8111
Unlimited Release
Printed September 2012

EFFECTS OF DEFECTS IN COMPOSITE WIND TURBINE BLADES: ROUND 2

Jared W. Nelson, Trey W. Riddle, and Douglas S. Cairns (Principal Investigator)
Department of Mechanical & Industrial Engineering
Montana State University, Bozeman, MT

Sandia Technical Manager: Joshua A. Paquette

Prepared by
Sandia National Laboratories
Albuquerque, New Mexico 87185 and Livermore, California 94550

Sandia National Laboratories is a multi-program laboratory managed and operated by Sandia Corporation, a wholly owned subsidiary of Lockheed Martin Corporation, for the U.S. Department of Energy's National Nuclear Security Administration under contract DE-AC04-94AL85000.

Issued by Sandia National Laboratories, operated for the United States Department of Energy by Sandia Corporation.

Available to DOE and DOE contractors from
U.S. Department of Energy
Office of Scientific and Technical Information
P.O. Box 62
Oak Ridge, TN 37831

Telephone: (865) 576-8401
Facsimile: (865) 576-5728
E-Mail: reports@adonis.osti.gov
Online ordering: http://www.osti.gov/bridge

Available to the public from
U.S. Department of Commerce
National Technical Information Service
5285 Port Royal Rd.
Springfield, VA 22161

Telephone: (800) 553-6847
Facsimile: (703) 605-6900
E-Mail: orders@ntis.fedworld.gov
Online order: http://www.ntis.gov/help/ordermethods.asp?loc=7-4-0#online

SAND2012-8111
Unlimited Release
Printed September 2012

Effects of Defects in Composite Wind Turbine Blades: Round 2

Jared W. Nelson, Trey W. Riddle, and Douglas S. Cairns (Principal Investigator)
Department of Mechanical & Industrial Engineering
Montana State University, Bozeman, MT

Sandia Technical Manager: Joshua A. Paquette

Abstract

The Wind Turbine Blade Reliability Collaborative (BRC) was formed with the goal of improving wind turbine blade reliability. Led by Sandia National Laboratories (SNL), the BRC is made up of wind farm maintenance companies, turbine manufacturers and third party investigators. Specific tasks have been assigned by SNL to the various parties. The portion of the BRC that will focus on establishing the criticality of manufacturing defects (aka, Effect of Defects) is being researched by the Montana State University Composites Group (MSUCG). The research described herein compiles the second round of a multi-year year plan consisting of three rounds of work performed by Montana State University (MSU) within two areas—Flaw Characterization and Effects of Defects. The first round was published in SAND2012-8110.[1] The purpose of this document is to capture and convey the progress which has been made by the MSUCG team since submission of the Round 1 Report.

The work presented has built upon the established framework for quantitative categorization and analysis of flaws. Additional physical testing has been performed utilizing improved manufacturing techniques that have reduced manufacturing time and materials, while providing samples with flaws common to wind turbine blades. This additional physical testing was performed to fill two needs: additional data points to further understand the Effects of Defects; and, to increase in scale away from simple coupons toward larger structures. These data were also analyzed to allow for continued analytical/experimental correlation occurring in this and future portions of this study. Manufactured specimens were evaluated non-destructively to verify flaw parameters and visualize damage utilizing computed tomography and digital image correlation, respectively.

A further understanding of the changes in the material properties associated with characterized flaws has been achieved on a coupon level with this additional physical testing. This testing further indicated that fiber misalignment and porosity resulted in decreased material performance. Modeling efforts toward matching these results have been performed utilizing two distinct and fundamentally different approaches. These are modeling damage as a degradation of properties, and modeling the actual damage in the material via finite element analysis with progressive damage. Reasonable agreement has been achieved when compared to the test data, though there is room for improvement.

Work will continue with efforts to increase size and scale of tested samples. In addition, research will be continued into reliability methods suitable for wind turbine composites. Finally, analytical/experimental correlation will be improved through the use of improved and more accurate models. This is leading to the goals of establishing the severity and criticality of manufacturing defects, and to provide a cogent approach to accept/reject criteria, and the need for repair and/or maintenance in the field.

Acknowledgements

The authors wish to acknowledge the help from Sandia contract monitors Dr. Daniel Laird (through March, 2011) and Mr. Joshua Paquette (current). The authors also wish to acknowledge technical help from Mr. Tom Ashwill and Mr. Mark Rumsey of Sandia.

In addition, the work and research presented herein could not have been performed without the assistance of the entire Montana State University Composites Group. Specifically, we wish to thank Dan Samborsky, Julie Workman, Daniel Guest, James Pallardy, and Cassidy Fisher for their direct contributions to this work. In addition, assistance from Edward Meehan, Patrick Flaherty, Pancasatya Agastra, and Matthew Peterson was paramount. Thank you!

Table of Contents

List of Figures

List of Tables

I. Introduction

The size, weight, shape and economic considerations of wind turbine blades have dictated the use of low cost composites materials. Even though composites have desireable engineering qualities, it is not apparent that design and manufacturing within the wind industry is able ensure a 20 year product life. Prevention of failures has been shown to have a profound economic impact on the continued development of the wind turbine industry. While significant research has been performed to better understand what is needed to improve blade reliability, a comprehensive study to characterize and understand the manufacturing flaws commonly found in blades has not been performed. The Department of Energy (DOE) sponsored Blade Reliability Collaborative (BRC) has been formed to perform such research.

Montana State University (MSU) has taken responsibility for the Effects of Defects portion of this collaborative and has split this into two distinct tasks: Flaw Characterization and Effects of Defects. The function of Flaw Characterization portion of this program has been to provide quantitative analysis for two major directives: (A) acquisition & generation of quantitative flaw data for use in the Effects of Defects numerical modeling program; and, (B) development of a flaw severity designation system for as built flaws. The Effects of Defects portion is focused on the development of modeling capabilities to predict the structural implications of common flaws found in composite wind turbine blades.

It must be noted that this work is intended to serve as a reporting effort on the preliminary development of data generated for use in a wind turbine blade reliability infrastructure. Testing and analysis are being performed on a specific material system and as such the absolute values presented are only valid for that particular system. However, the framework under development may be reproduced by interested parties on their specific material systems. Moreover, the probabilistic reliability and criticality/severity metrics being developed should be applicable to any composite structure assuming the requisite data is utilized.

Three composite material defect types (Figure 1) are being investigated through all rounds of this study after being deemed critical to blade function and life cycle: in-plane (IP) and out-of-plane (OP) waviness, and porosity/voids.[2] Many flaws are possible, but the flaws for this study were chosen via consensus of wind turbine blade manufacturers, wind turbine suppliers, wind turbine operators, and wind turbine blade repair companies. Initial results from these efforts was reported in Sandia Report SAND2012-XXXX.[1] These results included the first round of results from flaw surveys, non-destructive evaluation, flaw characterization, manufacturing, physical testing and damage modeling.

The work presented in the Round 1 report established that characterization of defects common to wind turbine blades is possible. A consistent framework was established and validated for quantitative categorization and analysis of flaws. With proper characterization, it is possible to establish the structural implication of a flaw. Applying the characterization techniques described in the Round 1 report to incoming data have enabled the generation of a statistically significant and comprehensive flaw database.[3] It is the goal of this investigation that these tools and data, once disseminated to industry, will contribute to improvements in the reliability of wind turbines.

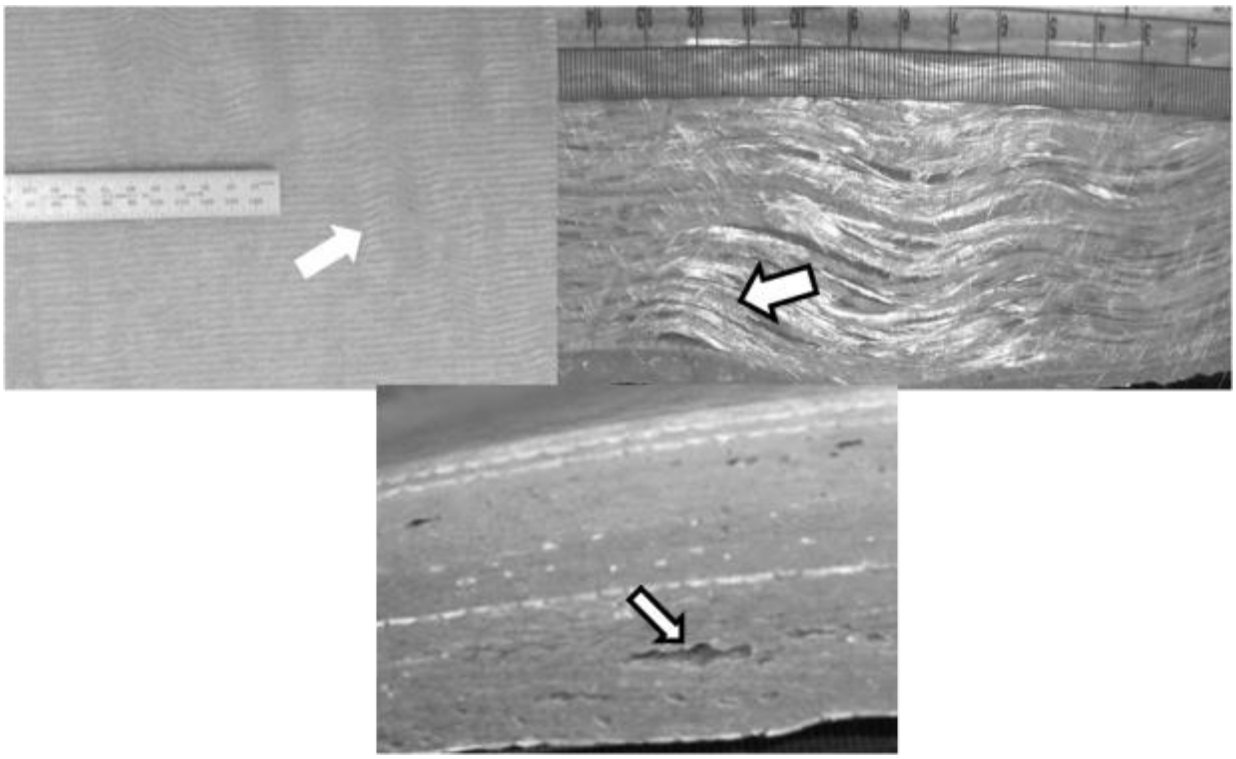

Figure 1: IP Waves seen on the surface (top-left); OP Waves seen through the thickness (top-right); and, Porosity/Voids seen within the laminate (bottom).

An understanding of the changes in the material properties associated with characterized flaws was achieved on a coupon level with physical testing performed in several configurations of the different flaw types.[4] This testing clearly indicated that fiber misalignment and porosity resulted in degraded material properties and decreased material performance. To compliment and work toward predicting these types of results, simple modeling efforts were performed and reasonable agreement was been achieved when compared to the test data.

The results and findings outlined in the Round 1 report culminated with a detailed outline of the critical functions to be undertaken during Round 2. These functions included improving analytical models, improving manufacturing techniques, additional static testing (in-plane and interlaminar), and further non-destructive evaluation. All of these functions were deemed necessary to improve the accuracy and ensure adequate representation of wind turbine blades. These next steps for this investigation were outlined in the Round 1 report and are copied below. This report outlines these next steps as well as future work for the continuation and completion of this study. Please note that for the proper and logical flow of this report, results are not presented in the order of the Round 2 Tasks listed below.

A. MSU EOD Round 1 Future Work Plan

1. Analytical model improvement
    a. Overall improved performance achieved and improved visualization of results established
    b. Exploration of utilizing explicit solver
    c. Continuum Damage Modeling (CDM) approach
        i. Established limits of 2d binary material property degradation model
        ii. Implemented initial softening methods to improve load-displacement curve accuracy
        iii. Initial 3d model generated and elastic testing performed

iv. Run models with properties from test data for convergence

d. Discrete Damage Modeling (DDM) approach
   i. Generated 3d mesh utilizing cohesive elements between tows and layers
   ii. Run models with properties from test data for convergence

2. Discussion of development of new manufacturing techniques that yield test articles which mimic more closely the defects observed in commercial wind turbine blades. Moreover significant effort has been undertaken to design fixtures which will enable the testing of thicker laminates. Reporting will include results of manufacturing and testing of thinner laminates that meet the following conditions:
   a. Improved manufacturing of porosity test articles and investigation of laminates with higher porosity content.
   b. Improved manufacturing of IP waveforms for better layer consistency and testing of flaw parameters missing from the Round 1 effort.
   c. Improve manufacturing process to more accurately match OP waves observed in blades and testing of flaw parameters missing from the Round 1 effort.
3. Multi-angle laminate testing and modeling
   a. Coupon size samples of [0, 45, -45, 0] tested in tension and compression
   b. Analysis of load-displacement curves for more complex behavior
   c. Model with binary material property degradation model to determine feasibility
      i. Binary material property degradation model eliminated from further use
4. Elimination of all ±45° laminates from further testing as results from Round 1 indicate that in most cases defect laden samples were not significantly degraded compared to controls. Whereas, 0° laminates were worst-case for all defect types and therefore warrant the full focus of this investigation.
5. Discussion of utilizing Non-Destructive Evaluation (NDE) technologies to verify flaw parameters and help with damage visualization. Preliminary results include use of computed tomography and digital image correlation during testing.

II. Improved Manufacturing Techniques

The Montana State University Composites Group (MSUGC) has identified the need to test laminates with embedded flaws. While methods utilized for Round 1 were satisfactory, improvements were made to reduce material waste, save manufacturing time, improve control and repeatability, and ensure flaws were as similar as possible to those found in wind turbine blades. To this end, several novel manufacturing methods have been developed and are outlined.

A. In-Plane Wave

IP waves are formed manually one ply at a time. The first step in the method of forming IP waves is to lay the fabric over a piece of polyethylene tubing oriented transverse to the 0° fiber angles in order to form a wave of approximately the desired amplitude and wavelength out-of-plane with the fabric. This is accomplished by pressing the ply gently over the tubing by hand, using only enough force to cause the tows to form around the tube. To ensure fiber integrity, this must be performed slowly due to the stiffness of the tows. Next, steel bars are placed on either side of the tubing to act as an anchor for the fabric when the hose is removed (Figure 2). Holding these steel bars in place by hand, the hose is then unclamped and removed (Figure 3). It is essential that the steel bars remain in place to constrain the wave through the entire process.

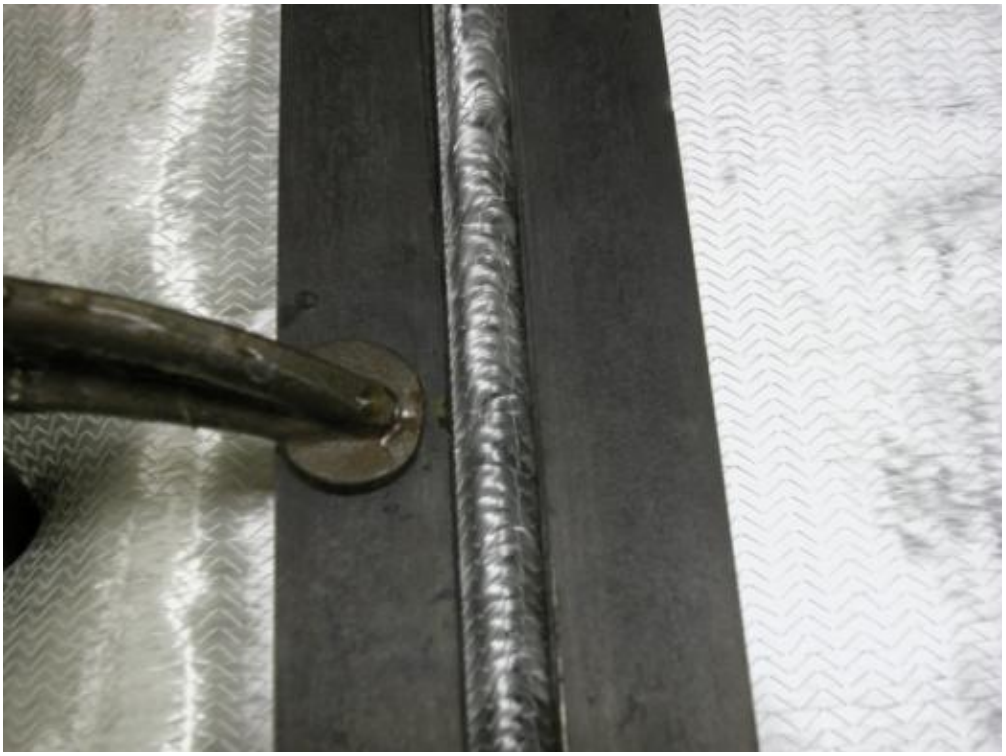

Figure 2: Fabric over polyethylene tubing constrained by steel bars.

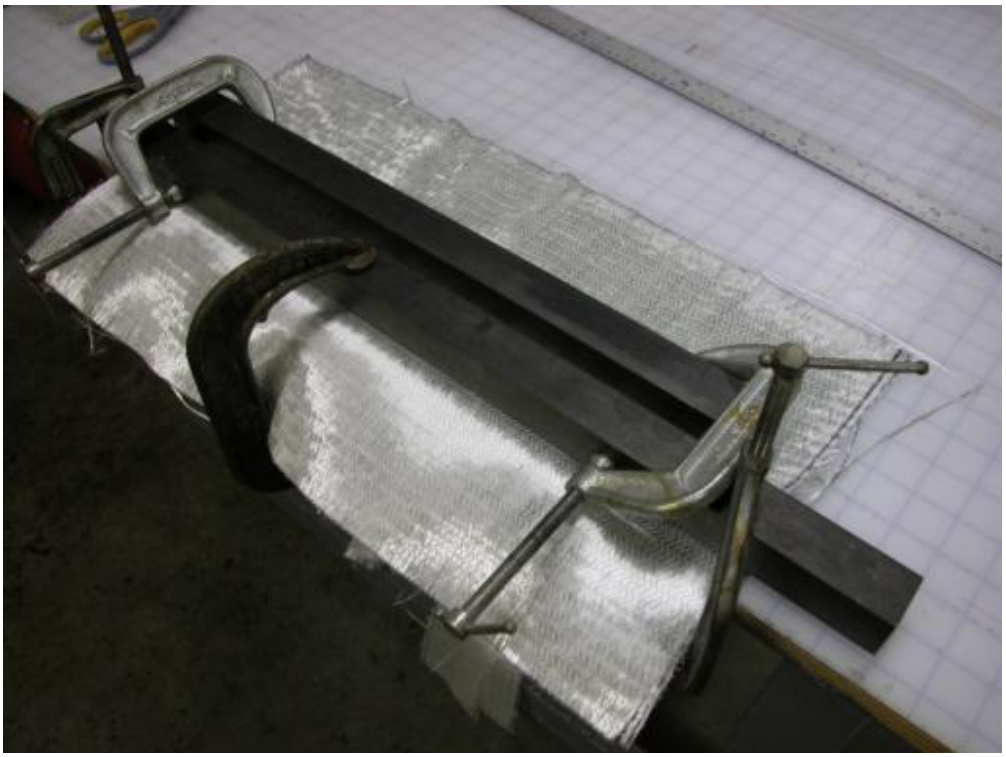

Figure 3: After the tubing is removed, the wave is ready to be pressed over into an IP wave.

Once the polyethylene tubing is removed the process of transforming the as-formed OP wave into an IP wave begins. First, the waves are manually pressed over, or essentially rotated to lay at approximately 45° to their initial out-of-plane orientation. Then the steel bars are removed and placed at a distance apart on the work table such that the fabric layer is laid between them so as to use them as end constraints for the tows (Figure 4). The partially formed waves are then manipulated further by hand, with care taken to keep the peaks of the waves aligned transversely to the 0° fiber angle and to prevent fiber wrinkling. Once the wave form has the approximate desired dimensions, the fabric is covered with 3/8" thick glass, while still remaining constrained by the steel bars (Figure 5). The purpose of the glass is twofold: first, the weight added friction between the fabric and the work table so that the wave form will remain as prepared for the time required to allow the tows to relax into the new form. Second, measurements can be made through the glass to get a rough estimate of the off axis fiber angle in the wave. The fabric must rest in this configuration for at least two hours allowing stresses in the fibers to be relieved. Once this is complete, the plies are stacked on the mold for the standard vacuum assists resin injection process.

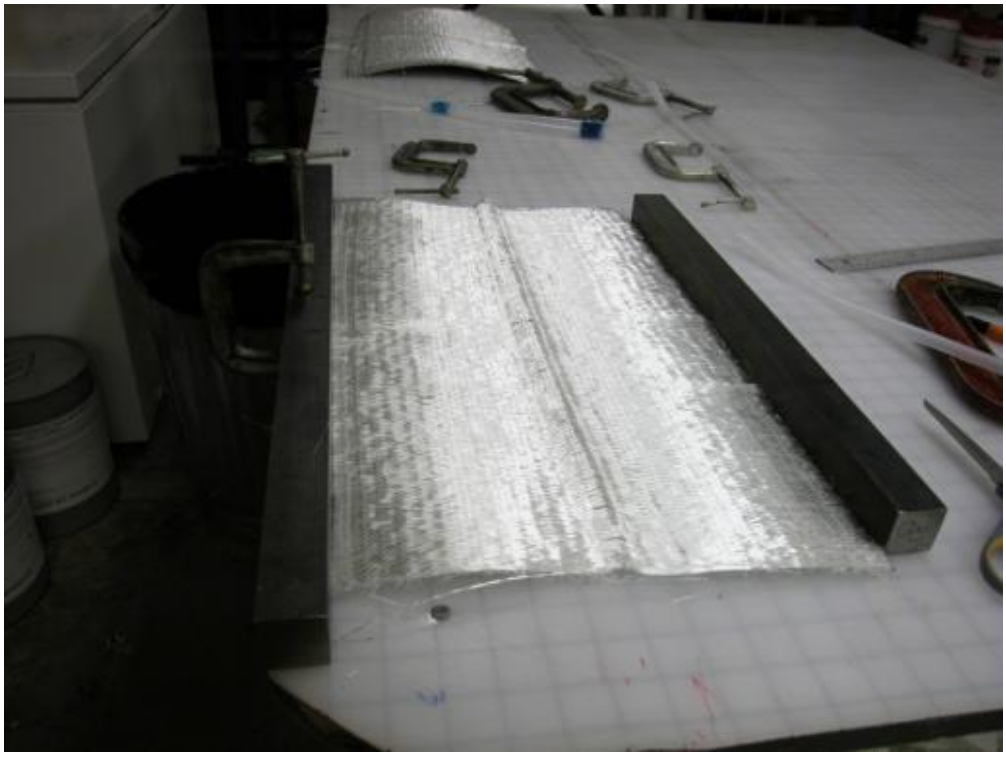

Figure 4: Partially formed wave constrained between steel bars.

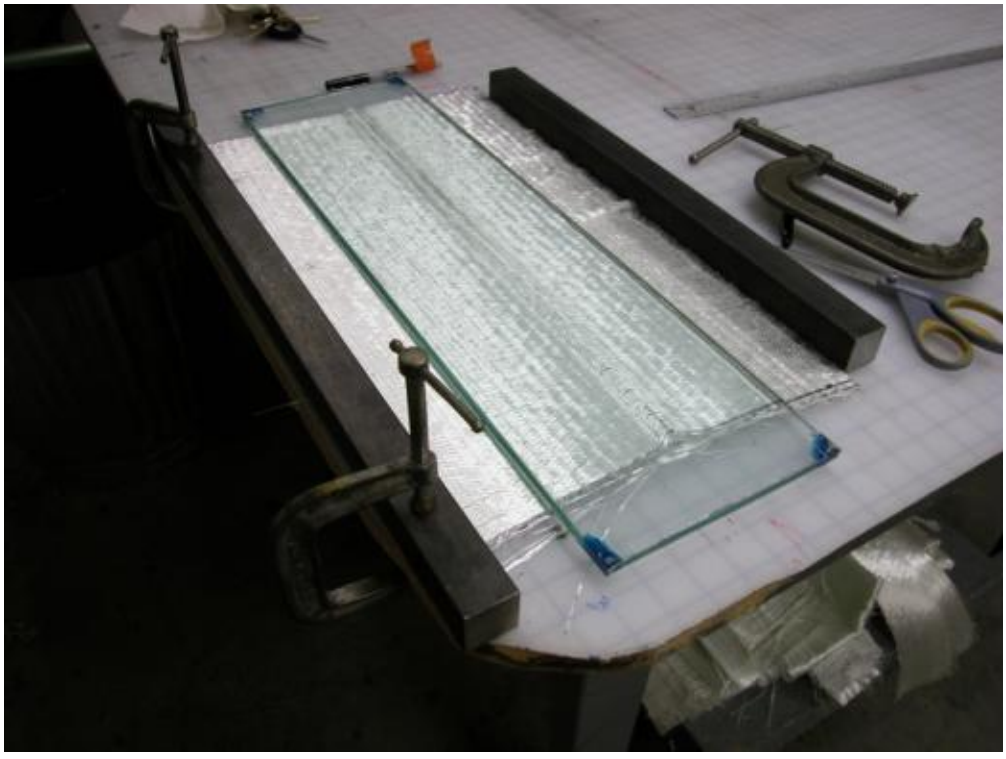

Figure 5: Finished wave relaxing under glass ready to be measured.

B. Out-of-Plane Waves

The first step in building a plate with OP waves is to secure the bottom layer of peel ply to the mold tool to ensure it does not shift during the infusion process. A form for the OP wave is then constructed using individual fiber tows. The fiber tows used for the wave build-up are cut to the width of the laminate. The wave build-up is created by stacking fiber toes in a pyramid fashion until the desired amplitude and wave length values are approximately reached (Figure 6). The OP wave sections are then placed onto the secured peel ply perpendicular to the direction of resin flow and to the orientation of the laminate fiber toes.

Figure 6: Chopped wave perturbation tows (top) and chopped tows as implemented for creation of OP waves (bottom)

Layers of fiberglass sheets are then placed on top of the mold while ensuring that the OP wave build-ups do not shift and remain perpendicular to the fiber direction. The buildup is completed by securing the top layer of peel ply and flow media. Once a vacuum is pulled, the OP wave buildups are rolled to ensure no air pockets or voids had formed. Infusion is then completed using a VARTM method (Figure 7).

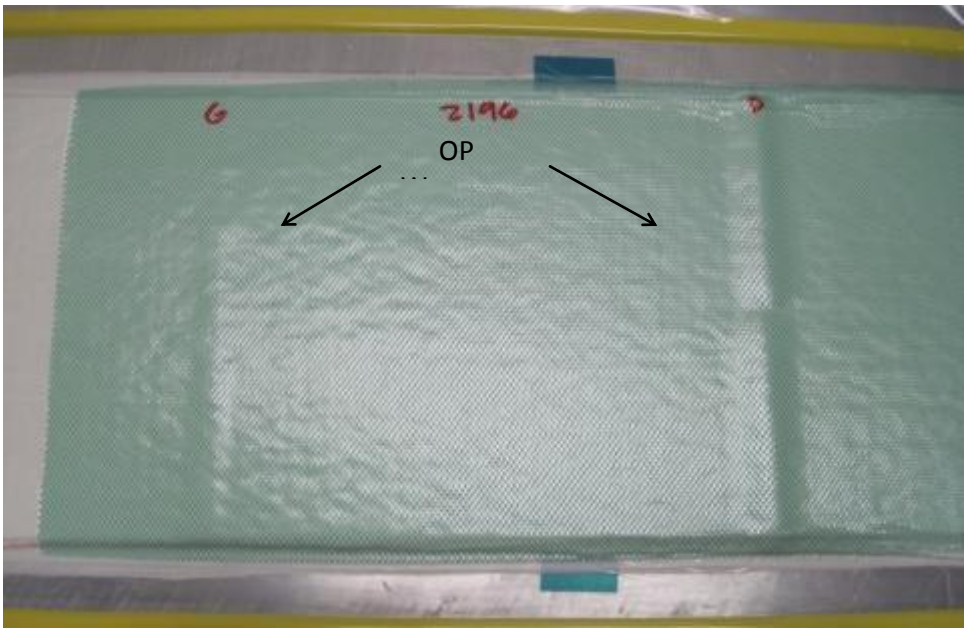

Figure 7: Plate under vacuum with OP waves

C. Porosity

A simple, yet effective, manufacturing process was developed for inducing porosity by introducing air into the plate while injecting resin. This method employs a "double bagging" technique which involves creating a 2" by 2" grid of holes in the first bag and then sealing that with a second bag. As can be seen in Figure 8, the second bag also has an inlet hose for letting air into the bag.

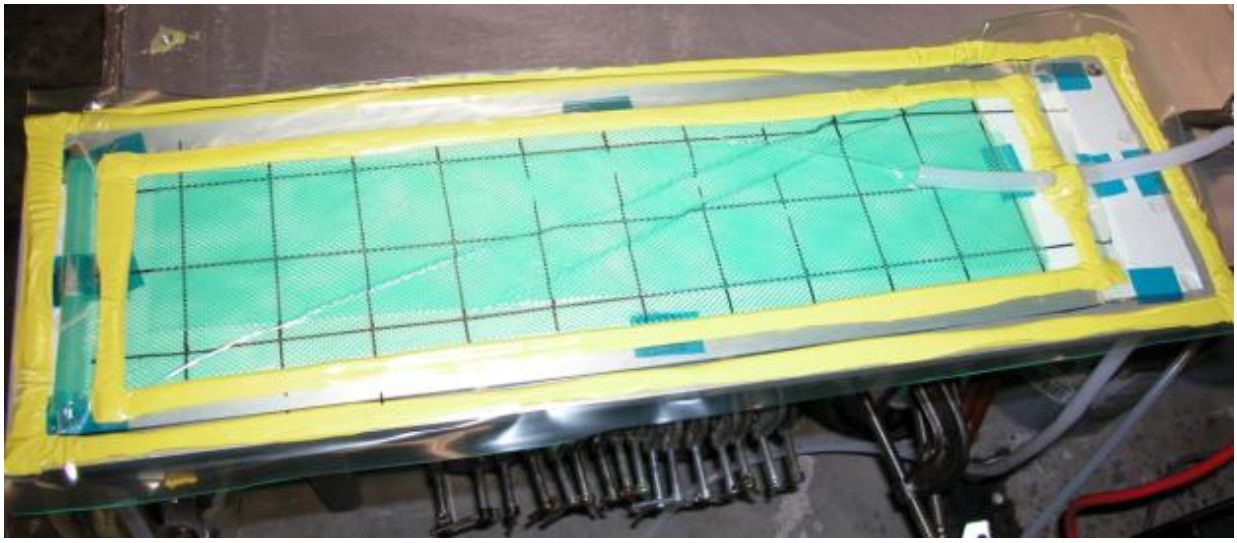

Figure 8: Double bagging with 2"x 2" grid of holes in first bag.

Trials with this approach have found that opening the inlet hose after the plate is infused results in low porosity contents. Higher porosity levels are achieved by allowing air to leak in slowly through the inlet hose during the entire infusion process. In short, when air is introduced during the infusion process, air becomes encapsulated in the laminate resulting in a porous laminate.

III. Non-Destructive Evaluation

As indicated in the Round 1 testing and evaluation, flaws introduced into the laminate changed during the manufacturing process. For example, it was noted that IP wave fiber angles changed resulting in an additional level of inaccuracy when analyzing the results and performing analytical/experimental correlations. Thus, due to variability in the manufacturing processes, it is necessary to characterize the as-built flaw parameters prior to testing to ensure that all analyses are performed accurately.

A. Waves

Previous work has concluded that waveforms found common to wind turbine blades follow sinusoidal geometric periodicity and are mechanically best characterized by off-axis fiber angle. The method for extracting this information remains the same as outlined in the Round 1 Report.[1] Through thickness, IP wave images for each layer are collected with the use of a Computer Tomography (CT) scanner. With this technique wave parameters (amplitude and wavelength) for each ply can be measured, while OP waves can be measured by hand. Figure 9 shows an example of an IP wave image collected from the CT scanner.

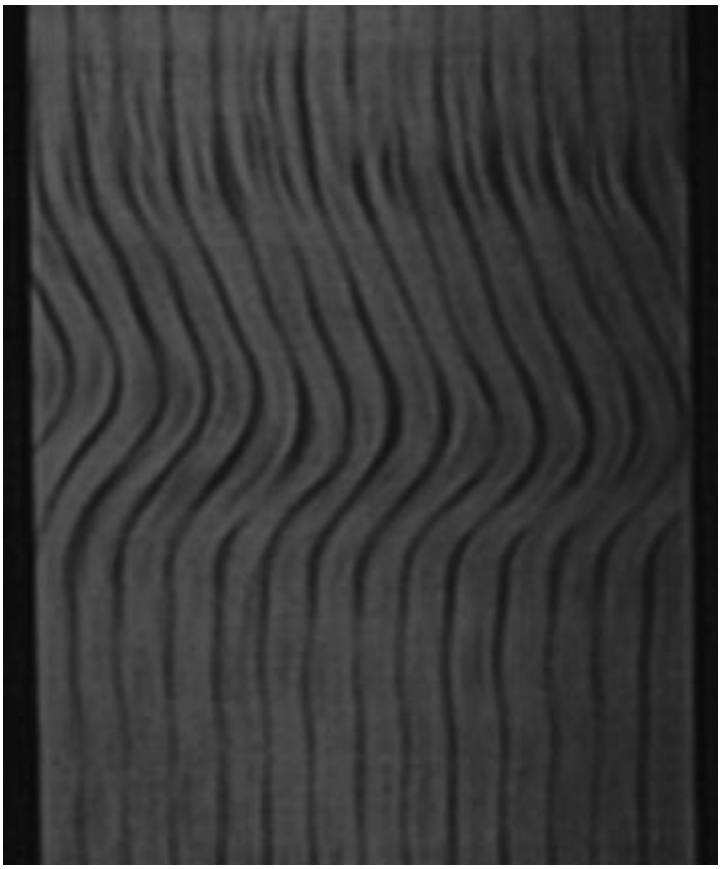

Figure 9: Radiograph of an IP wave

Analysis of the as-built waveforms confirmed improved manufacturing consistency associated with the process improvements described in detail in Section II.A. This was evident not only by less variability between layers but waveform parameters were closer to intended target values.

B. Porosity

The method employed by the Montana State University Composites Group for obtaining porosity content values with the most success is microscopy. For this process specimen are cut into small pieces, mounted in acrylic resin and then polished. Depending on the size of the voids either an optical or Scanning Electron Microscope (SEM) is used to take digital images of the cut surface plane. Image processing techniques are then used to identify the location and size of gas inclusions. From this data a planar area fraction of porosity content is established. This value is then extrapolated to percent porosity by volume. An image taken by a scanning electron microscope on a specimen with induced porosity is shown in Figure 10. This process proves to be time consuming and has the potential for mistakes to be made by the investigator.

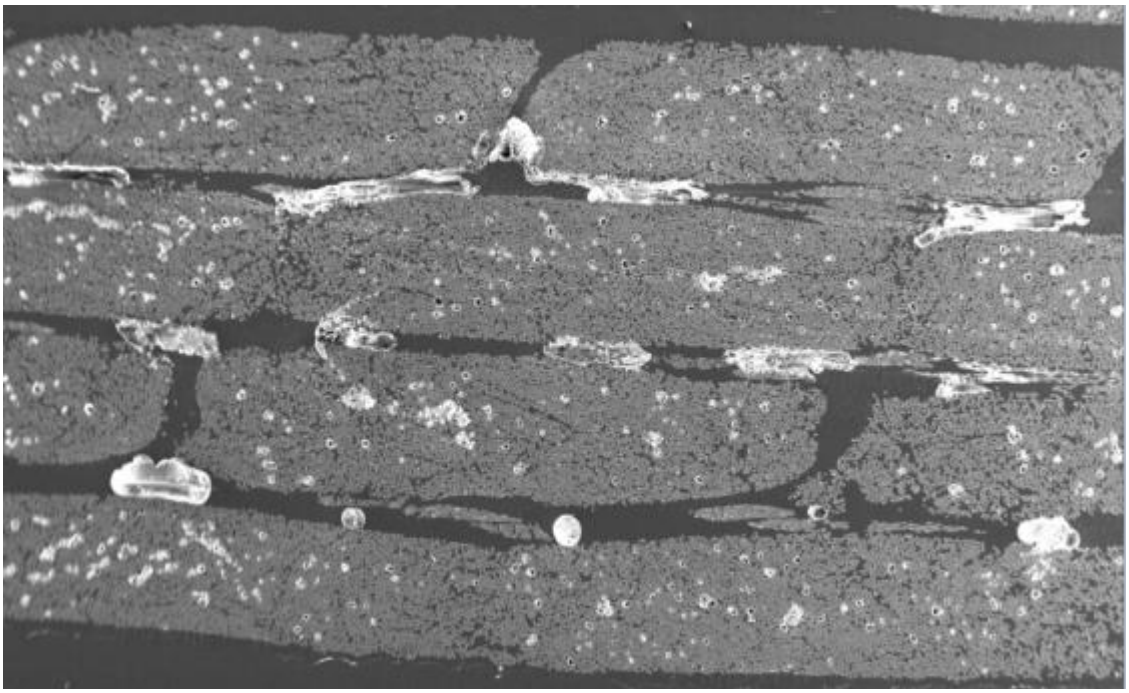

Figure 10: Laminate with porosity

A novel method for characterizing porosity in composite laminate plates is under development. Preliminary results show that there is a good correlation between radiodensity and percent porosity by matrix volume (Figure 11). Radiodensity is a measure of the linear attenuation of X-rays and is related to both the density and atomic number of a material. Measuring radiodensity is quick and easy to do with an X-ray machine and as these devices become more portable, this technique may prove to be an inexpensive and efficient way to evaluate porosity in the field and on the manufactures floor.

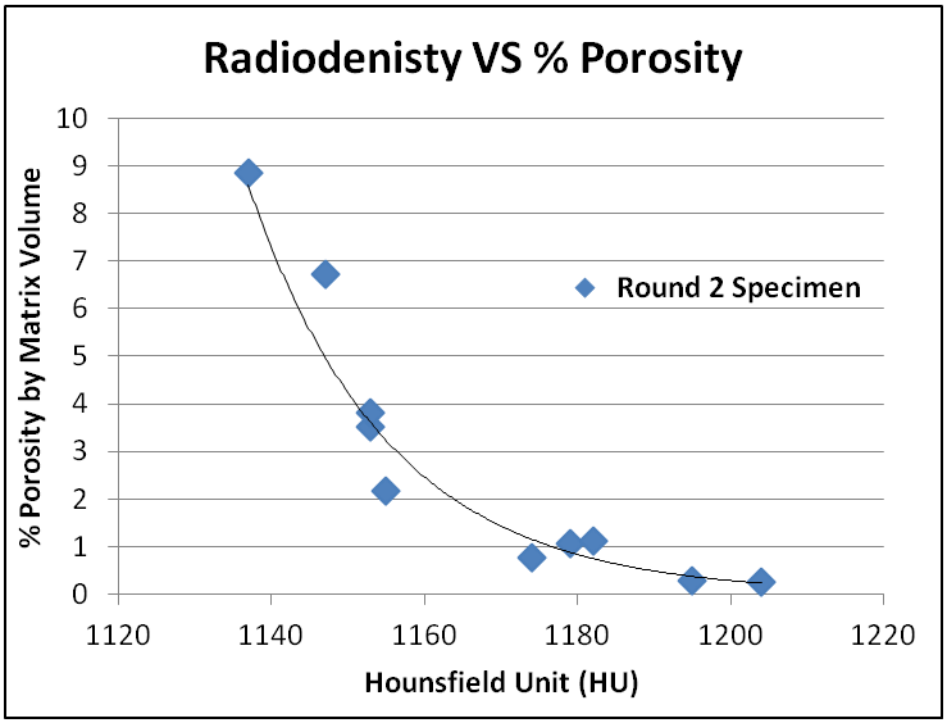

Figure 11: Correlation between porosity and radiodensity

The Hounsfield Scale is a quantitative scale for describing the linear attenuation of X-rays through a material. By definition, distilled water and air at standard atmospheric pressure and temperature have values of 0 and -1000 Hounsfield Units [HU] respectfully.[2] The CT scanner can measure the attenuation of the scanned material and calculate the radiodensity in relationship to air and water using the following equation:

$$HU = \frac{\mu_x - \mu_{water}}{\mu_{water} - \mu_{air}} \times 1000 \quad (1)$$

Where μ_x, μ_{water} and μ_{air} are the linear attenuation coefficients for the material under inspection, distilled water and air respectively. As Steve Nolet (Principal Engineer & Director of Innovation of TPI Composites) indicated to this project team, there is a need in industry to develop effective methods quantify levels of porosity and its effects on laminate mechanical response:[3]

"Porosity is a HOT BUTTON top for TPI. It affects our operations not because of field failures, but primarily because of the inability to characterize levels of porosity in a part (accurately) AND project its effect on long term service. As a result, we believe, a significant amount of rework or scrap is created without any basis. Rework usually involves the removal of three to seven times more GOOD laminate than porosity affected laminate as a result of required scarf angles for repair (often 20:1 or 50:1).

So this work is really important to us, but it also needs to be accompanied by a comprehensive methodology to characterize the void content in a production blade using non-destructive techniques. We have had difficulty establishing procedures to accomplish this (percentage and depth of porosity, included!).

I will solicit input from the other individuals from TPI that I have copied and we will likely want to engage in a more detailed discussion as we provide you with the information you have requested below. It may very well make sense to plan on a meeting with [your group] to really flesh this issue out and build a program that will service the blade manufacturing community in a significant way."

IV. Round 2 Physical Testing

Physical testing is necessary for the establishment of damage growth and validation tools of composite wind blades to contribute toward a reliability infrastructure for the wind industry. The goal of the Round 2 test program was to further characterize the mechanical properties of the critical defect types and the results are presented herein. In addition, as with the Round 1 results, all Round 2 results were utilized for analytical/experimental correlations, with the purpose of performing laminate analysis with included defects.

A. Materials and Processing

Generally, laminates were infused utilizing a VARTM process with one layer of peel-ply on the top and bottom surfaces and one layer of flow medium on the top surface of the laminate except where noted in the manufacturing procedures above. Mostly uni-directional PPG-Devold 1250 gram-per-square-meter E-glass was used with a Hexion RIM 135 resin system in all cases. Laminates were manufactured with all fibers in the 0° direction with the exception of the Multi-Angle testing which had fiber directions of [0°,+45°,-45°,0°]. The cure profile for each panel was 48 hours at room temperature followed by 8 hours at 70°C. The nominal fiber volume fraction of the panels was 55% with a nominal thickness of 0.8 mm for each layer.

Test coupons were cut from the panels for use in tension and compression testing. Tensile coupons were cut to approximately 50 mm wide by 200 mm long and were tabbed resulting in a gage length of 100 mm. Compression coupons were cut to approximately 25 mm wide by 150 mm with an anticipated gage length of 25 or 38 mm where the wavelengths were greater than 25 mm. Larger scale test coupons were cut and machined as well and are outlined in more detail below.

In addition, specimens were manufactured for delamination testing. During the infusion process, a layer of release film was placed at the mid-plane of the four-ply laminate to create an initial crack 25 mm in length from the leading edge. Coupons were cut to a width of 25 mm and aluminum pull-tabs (blocks) were bonded to the end with the initial crack. Coupons for double cantilever beam (DCB) testing were cut to a length of 150 mm, while those for end-notch flexure (ENF) testing were cut to 100 mm to fit existing MSUCG fixtures.

B. Test Methods: Static In-Plane and Delamination

Coupons were constructed with representative blade materials and construction processes though scale was reduced. Scaling was required to achieve compatibility with the Instron 8802 250 kN testing machine and grip capacity (Figure 12). Static ramp tests on the specimens were conducted at a rate of 0.05 mm/s in tension and 0.45 mm/s in compression for all 4-ply coupon and Multi-Angle laminates. Typical of the Montana State University Composites Group (MSUCG), tensile these tensile tests were performed based on the ASTM D 3039 tensile testing of composites standard.[5] This simple test can be used to find the ultimate tensile strength and strain, tensile modulus, Poisson's ratio and transition strain. Likewise, compression testing is more loosely based on ASTM D 3410 and D 6641.[6,7] Properties that may be derived include ultimate compressive strength and strain, compressive modulus and Poisson's ratio in compression.

Failure within composite materials commonly occurs as the result of delamination and significant work to understand the strain energy release rates has been performed. This type of defect and damage was added to the initial IP waves, OP waves and porosity in Round 2 testing and analysis. Noting this, calculations to determine whether a crack will propagate can be performed. Further, with residual strength and damage propagation characterized, determinations of a laminated, and perhaps a blade's, damage tolerance can be made.

Figure 12: Representative tensile (left) and compressive (right) samples being tested.

Given this common type of failure of composite materials, many tests exist to characterize interlaminar fracture. Generally, test methods are used to determine a critical strain energy release rate for crack propagation, G_C. This critical value must be experimentally determined for each material system as well as for each mode. In practical terms, materials that are "tougher" have higher critical values of G_C, requiring more energy to grow a crack in that material. For both Mode I and II tests outlined below, visual crack length techniques were utilized by measuring the crack length on each side and then utilizing the average value. This is particularly useful in the run-arrest growth scheme observed in these tests.

The standard test for Mode I is the double cantilever beam (DCB) as described in ASTM standard D5528 and shown in Figure 13 where opening forces are applied to the ends of the speciman.[8] The critical strain energy release rate (G_{IC}) to grow a crack in the material is determined from the load-displacement curve of the test and the modified beam theory method. From this, the Mode I (opening) interlaminar fracture toughness may be calculated. It is worth noting that initially the G_{IC} increases monotonically before stabilizing, due to fiber bridging that increases the fracture toughness of the specimen. Values calculated beyond the end of the initial crack may be considered dubious and thus, the initiation value is preferred.

Figure 13: Double Cantilever Beam (DCB) specimen just prior to first Mode I crack propagation.

The end-notched flexure (ENF) test has emerged as the standard test method for measuring Mode II (shearing) type crack growth within the MSU Composites Group.[9] Specimen geometry and loading for an ENF specimen are shown in Figure 14. This specimen produces shear at the mid-plane of a composite loaded in three-point bending and at critical load the crack advances. The strain energy release rate (G_{IIC}) to grow a crack in the material is determined from the load-displacement curve of the test and the modified beam theory method. From this, the Mode II interlaminar fracture toughness may be calculated.

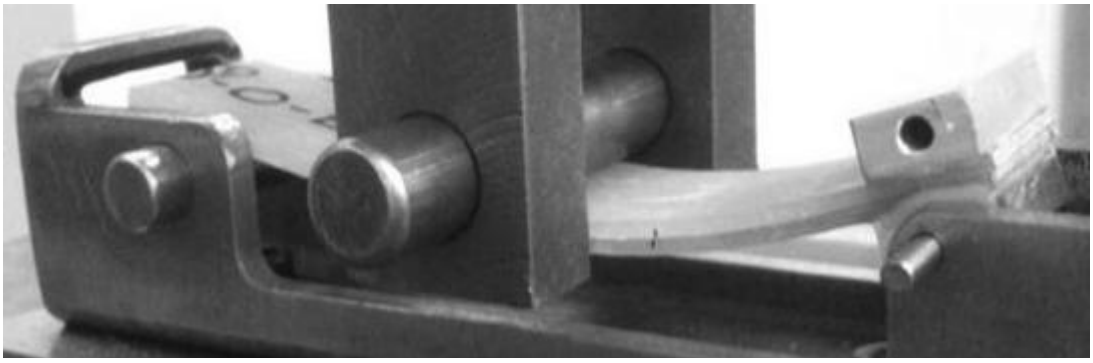

Figure 14: End-Notch Flexure (ENF) specimen just after Mode II crack propagation.

A total of approximately 50 coupons were tested with 3-5 in each test group. Results of all experiments will be available in the DOE/MSU Composite Material Database.[4]

C. Thin Flawed Laminate Testing Results

Review of Round 1 testing showed gaps in the data, e.g. no fiber angles between 0 and 15deg, porosity values <2% etc.[1] Moreover some of the results, in particular from the OP waves were considered to dubious. It is the goal of this program, to be able to accurately predict the Effects of Defects in thicker laminates such as those found in wind turbine blades. However testing of thick laminates for model validation is resource intensive, therefore only a small number of larger scale tests will performed. The purpose of these larger tests will be to validate the extrapolation of models developed on thinner laminates to larger ones. The need for generating a comprehensive flawed material properties dataset coupled with improvements in manufacturing techniques provided the impetus for continued thin laminate testing.

Raw results from these tests are provided in Tables 6-8 and may be found in Appendix VII. A. . These provide data at a much wider range of the key variables for each flaw type allowing for more insightful analyses to be performed as below. In addition, these data were utilized to provide load-displacement and stress-strain curves, also found in Appendix VII. B. . These will be of particular use in continuing correlation to analytical models.

Analysis of the results show that strength degradation in laminates with waves tend to correlate slightly better to the average fiber angle of all layers rather than the maximum fiber angle. Figure 15 &Figure 16 display the results of failure stress verses average fiber angle for IP and OP wave respectively. Results from compression of OP waves is not being presented as they are still under investigation. An OP wave embedded in a planar structure under compression is inherently an eccentricity and is therefore subject predominately to buckling. While buckling is a common mode of failure in a wind turbine blade it is driven in large part by the global structure and local geometry. With this in mind, care must be given to ensure that the failure data, from a material standpoint, is completely understood. In analysis of the effects of porosity on laminates it is necessary to consider the variations in the fiber volume ratio. As porosity increases, one of two things must happen as a direct function of encapsulated gases; the volume of the part must grow (typical for vacuum bag manufacturing) or should the total volume remain the same (typical of cull plate manufacturing), there must be a reduction of resin content. Either case will cause variations in the fiber volume ratio. Test specimens in the investigation have been manufactured using a vacuum bag technique therefore it is necessary to include volume effects. A simple method for comparing results in this case is to normalize the failure stresses to 55% fiber volume ratio, V_f. Figure 17 shows a comparison between porosity content and the reduced strength.

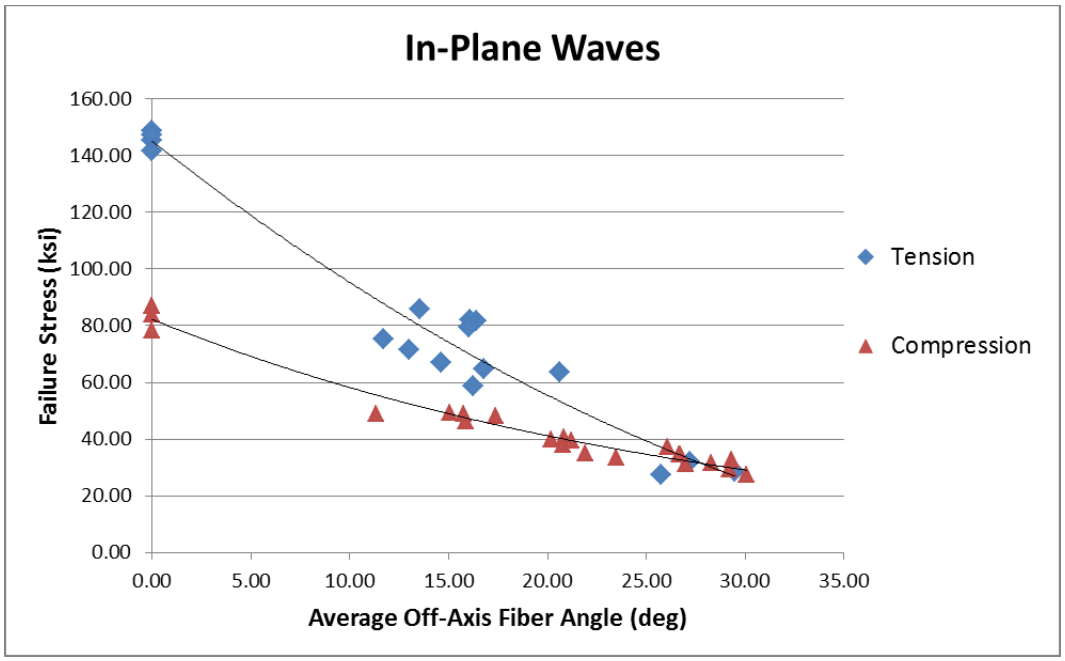

Figure 15: Peak Stress of IP Waves at various fiber angles.

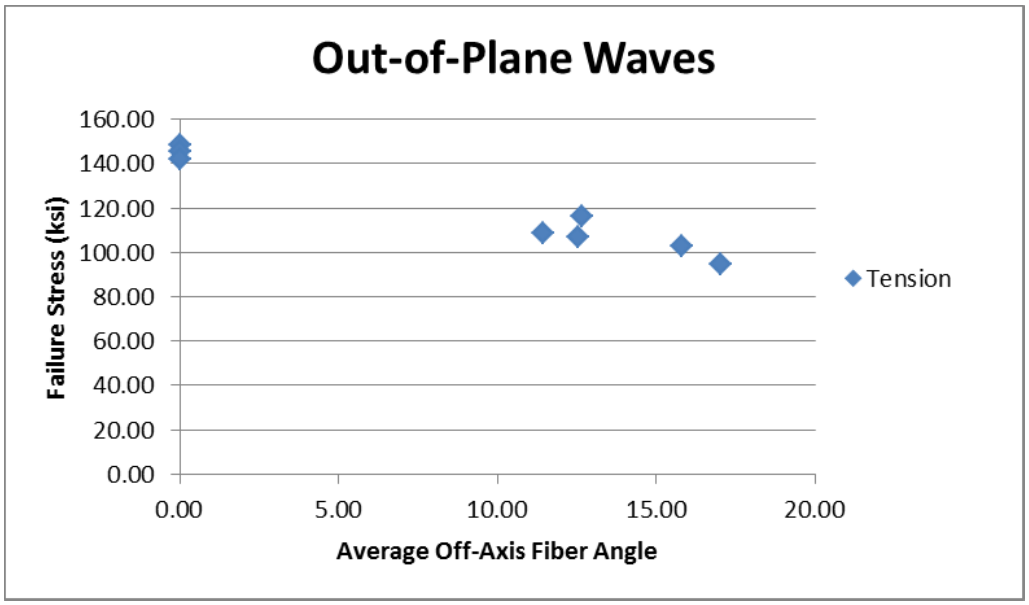

Figure 16: Peak Stress of OP Waves at various fiber angles.

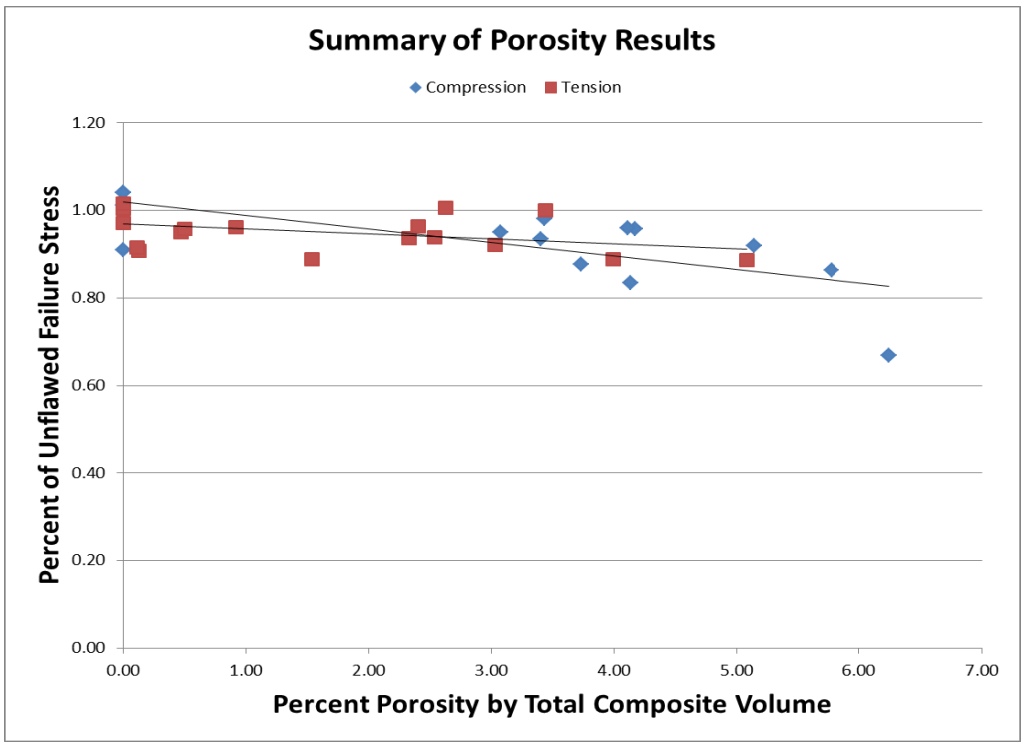

Figure 17: Reduction in Strength due to porosity.

The data in Figure 17 report the as-measured experimental data from mechanical tests. The void content was determined by image analysis of specimens from the same plates which were used for the test coupons. The void data are presented as a function of void content in the composite to provide use to designers on that basis.

Some discussion on the micromechanics of voids in the composite is warranted. The influence of voids on the mechanical properties has the effect of reducing the bulk modulus of the resin. While this does

not have as great of an effect in tension, the reduced modulus has a significant effect for compression strength as the reduced modulus does not support the fibers in compression as well as a stiffer matrix.

The first model for resin modulus reduction might be based on the rule of mixtures:

$$E_m' = E_m (1-V_v) \quad (2)$$

Where E_m' is the reduced matrix modulus of elasticity,
E_m is the modulus of elasticity of the matrix without voids, and
V_v is the void volume fraction

However, a void, modeled as a spherical inclusion reduces the matrix modulus of elasticity to a greater extent than simple rule of mixtures because of the local strain concentrations from the spherical void geometry.[10-12] Additional studies, outside the scope of this report may be necessary to apply these data to other material systems to predict the influence of void content on mechanical properties.

The results of this testing effort have been considered in large part to be a success. In particular, a comparision was made with a study on compression of fiberglass composites containing pororsity performed by BRC member TPI.[13] Both the TPI and MSUCG data sets are depicted in Figure 18 where strong correlations between the two can been seen. In general, correlation of ultimate strength to flaw characterization parameters exhibit trends describable through regression with values for coefficient of determination greater than 0.9. Moreover model predictions of load displacement curves are expected to be accurate to within ±5%.

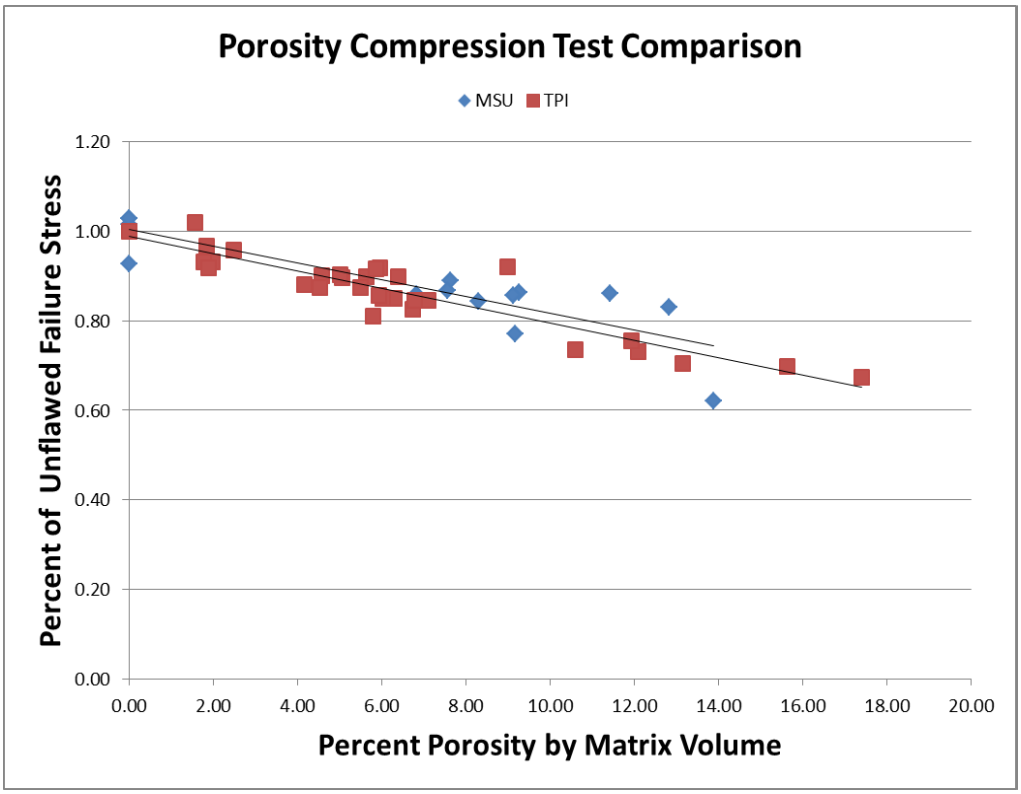

Figure 18: Comparision of results from compression testing of specimens containing prosity.

D. Multi-Angle Laminate Physical Testing and Results

As noted in the Round 1 report, Multi-Angle laminate testing was suggested to enable analytical and experimental correlation with a more complex load-displacement curve. In short, the more complex laminate would likely have more damage accumulation through the test which would require a higher level of accuracy from associated models.

i. Multi-Angle Laminate Tension Results & Discussion

Tensile tests were carried out on Multi-Angle laminates with fiber orientation of [0°,+45°,-45°,0°] with no intentional defects introduced. Material properties were calculated (Table 1) as outlined by ASTM D 3039 which was used as a guideline for this testing and resulting analysis. Load-displacement and stress-strain curves for each test are shown below in Figure 19 & Figure 20. Peak load and strain-at-failure was fairly consistent with differences of approximately 3% and 12%, respectively. The peak average stress of approximately 0.56 GPa was lower than 1.02 GPa noted in Round 1 testing.[1] This is easily explained with the change to the Multi-Angle laminate from the uni-directional laminate used in the Round 1 testing. While it was intended that the load-displacement curves would be significantly more complex, Figure 19 confirms that only two significant changes: increased softening up to initial failure and then a short load plateau before ultimate failure. Further discussion of these salient observations may be found below .

Table 1: Multi-Angle laminate tension material properties.

Ultimate Strength	81.0	ksi	558	MPa
Maximum Stress	81.4	ksi	561	MPa
Strain at Failure	5.09	%	--	--
Modulus of Elasticity	2.42	Msi	16.7	GPa

ii. Multi-Angle Laminate Compression Results & Discussion

Based on the same logic for performing the tensile tests above, compressive tests were carried out on Multi-Angle laminates with fiber orientation of [0°,+45°,-45°,0°] with no intentional defects introduced. Material properties were calculated (Table 2) as outlined in several ASTM standards that were used as a guidelines for this testing and resulting analysis. Load-displacement and stress-strain curves for each test are shown below in Figure 21 &Figure 22. Peak load and strain-at-failure was fairly consistent with differences of approximately 3% and 12%, respectively. Likewise, the peak average stress of approximately 0.32 GPa was lower than 0.58 GPa noted in Round 1 testing.[1] This is easily explained with the change to the Multi-Angle laminate from the uni-directional laminate used in the Round 1 testing. Below, Figure 21 confirms the same two significant changes from the uni-directional tests in Round 1: increased softening up to initial failure; and, a short load plateau before ultimate failure. Similar to the tensile tests, a damage progression section is noted in the curves between the initial failure and ultimate failure allowing for more accurate assessment of experimental and analytical convergence. Further discussion of these salient observations may also be found below.

Table 2: Multi-Angle laminate compression material properties.

Ultimate Strength	46.0	ksi	317	MPa
Maximum Stress	45.2	ksi	312	MPa
Strain at Failure	0.83	%	--	--
Modulus of Elasticity	6.49	Msi	44.8	GPa

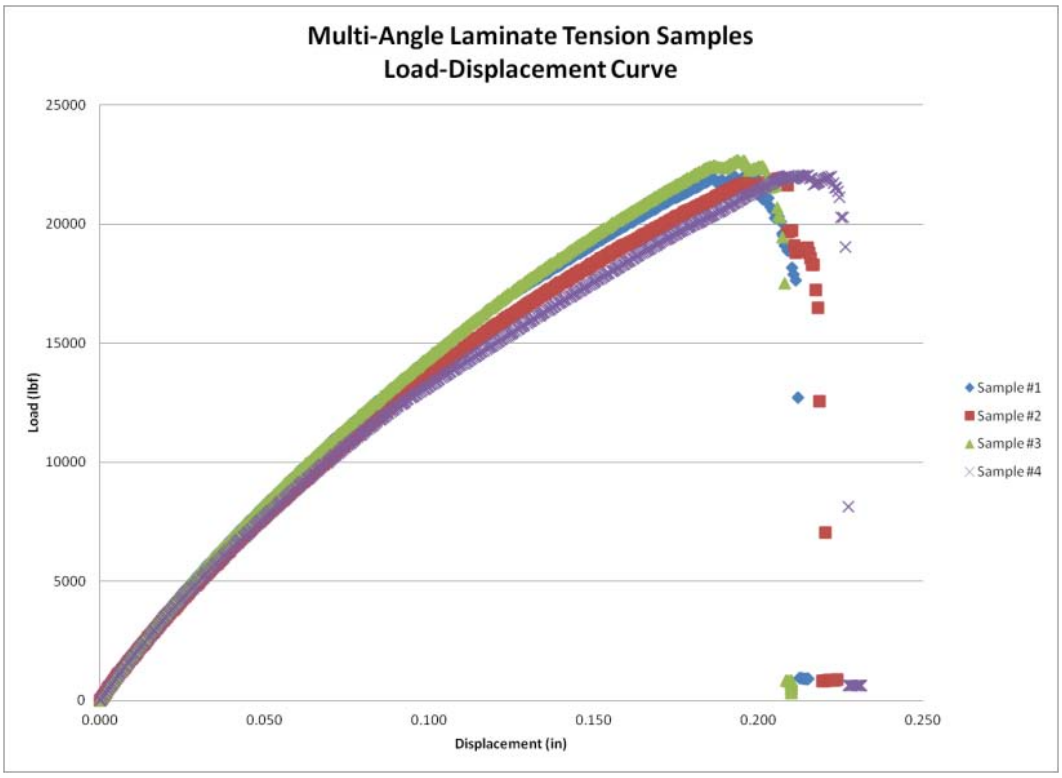

Figure 19: Multi-Angle laminate tension testing load-displacement curves.

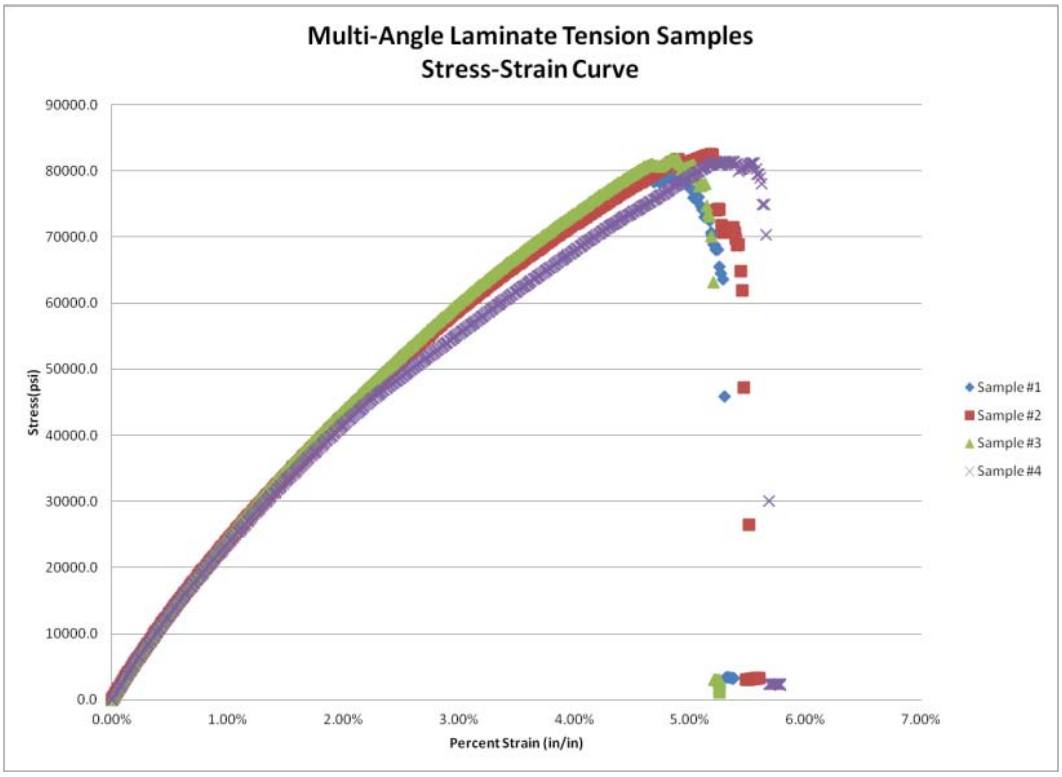

Figure 20: Multi-Angle laminate tension testing stress-strain curves.

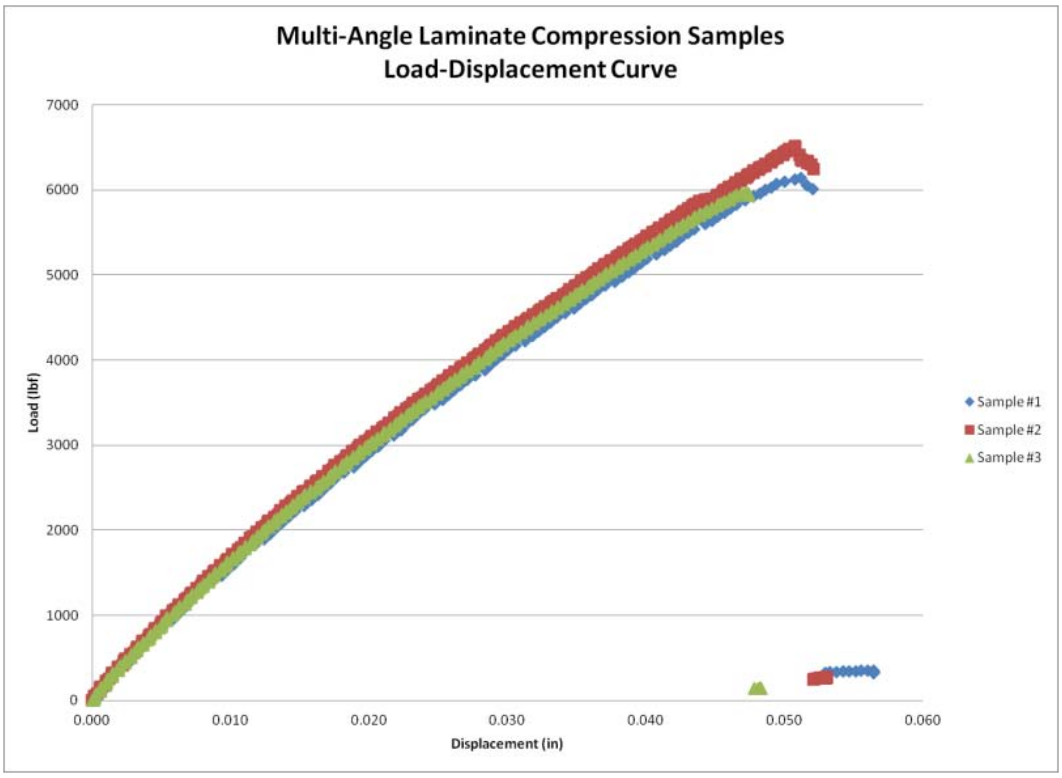

Figure 21: Multi-Angle laminate compression testing load-displacement curves.

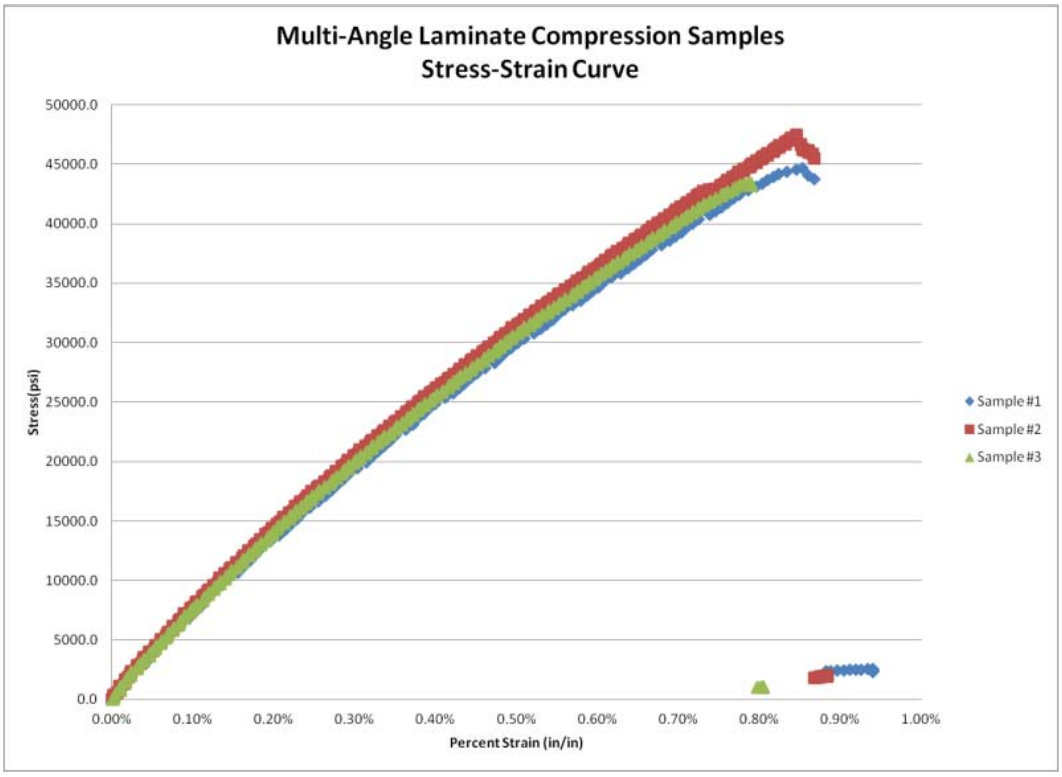

Figure 22: Multi-Angle laminate compression testing stress-strain curves.

E. Delamination Testing Results & Discussion

As noted above, delamination damage analysis of composites is common and widely performed due to much lower strengths compared to in-plane. Failure occurs as the result of delamination, which must be considered as part of an accurate analytical tool. This is especially true for discrete damage modeling where cohesive elements are placed between layers so that crack propagation may occur not only within the layer, but also between layers. This discrete approach is discussed in more detail below. Also as noted above, DCB and ENF tests were performed to determine critical strain energy release rates in Mode 1 and Mode 2, respectively.

An increasing crack resistance behavior is noted due to fiber bridging as the crack propagates through each sample (Table 3). This result is expected and is due to secondary cracking and fiber bridging. Only initial cracking was considered for ENF testing and these values are found below in Table 4. Representative load-displacement curves may be found below (Figure 23 & Figure 24). Initial values are fairly consistent and appear reasonable for use in delamination prediction in future modeling efforts as outlined below. Data was collected utilizing a primarily 0° uni-directional material to attain the lowest possible values for G_{IC} and G_{IIC}. Thus, results are conservative when applied to cases with other fiber angles. These data will be particularly useful going forward with complex modeling efforts for analytical/experimental correlation, specifically with discrete damage modeling as outlined further below. However, no additional delamination testing is planned and will only be pursued further if deemed necessary to further the modeling efforts.

Table 3: Mode I critical strain energy release rate determined from DCB testing.

Sample	Initial GIc	Secondary GIc	Final GIc	Units
DCB_01	295	506	720	J/m^2
DCB_02	287	651	854	J/m^2
DCB_03	320	659	843	J/m^2
AVERAGE	301	605	806	J/m^2

Table 4: Mode II critical strain energy release rate determined from ENF testing.

Sample	GIIc	Units
ENF_01	1321	J/m^2
ENF_02	1883	J/m^2
ENF_03	1367	J/m^2
AVERAGE	1524	J/m^2

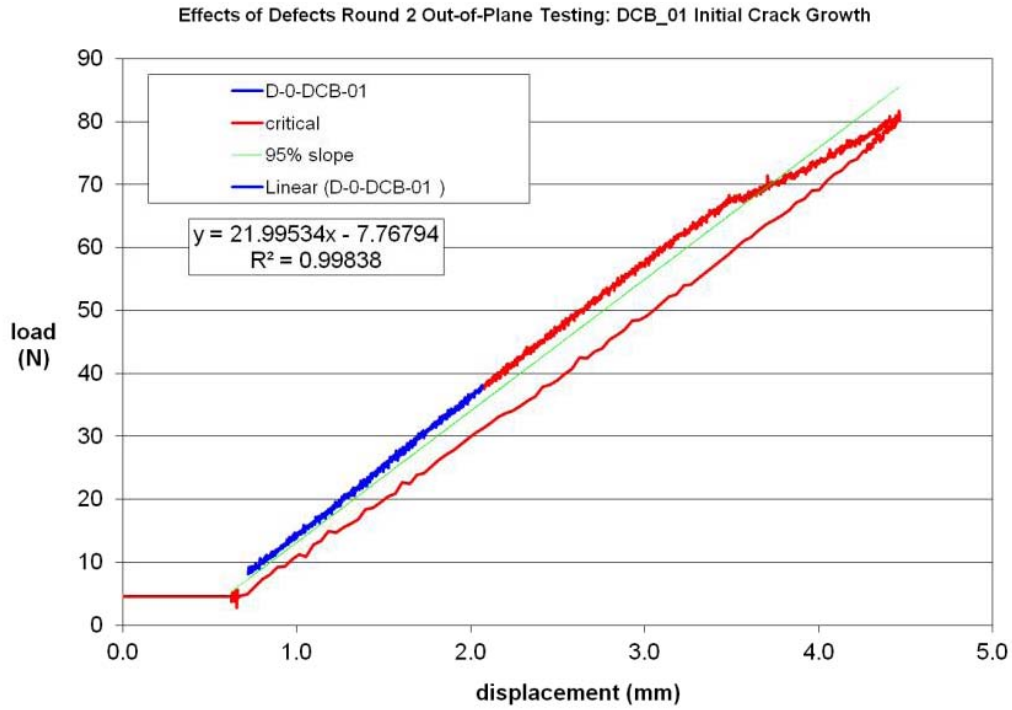

Figure 23: Representative load-displacement results from a Double Cantilever Beam (DCB) test during initial crack growth.

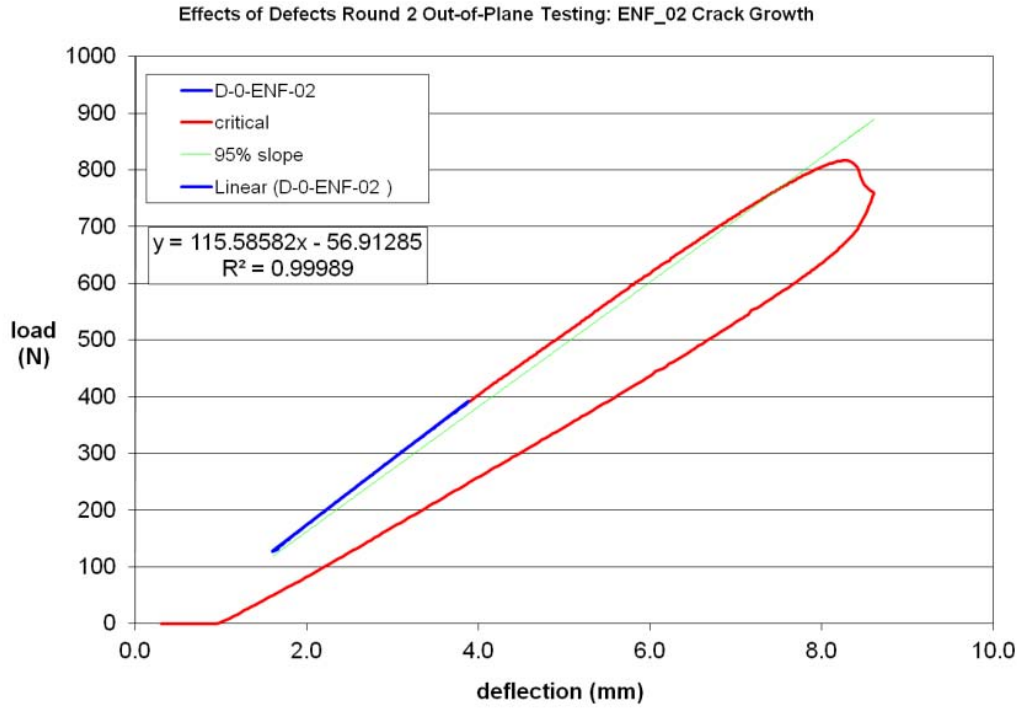

Figure 24: Representative load-displacement results from a End-Notch Flexure (ENF) test during crack growth.

F. Thick Specimen Testing

Wind turbine blades are primarily composed of thick composite laminates (>1 in). While prior research has shown strong tendencies for laminate mechanical response to scale according to Weibull scaling theories (critical defect sensitivity), there is no conclusive evidence to support that the response of flawed structures will follow the same trends.[14] Therefore, it was decided to test thicker layups. In order to complete this task, new testing fixtures had to be designed and manufactured for use in high load test machines. Brief outlines for the fixtures designed for both tension and compression are given below and manufacturing drawings are available upon request.

i. Tension Fixture Development

Tension testing is being performed on a Baldwin 200kip hydraulically actuated test machine. Grips on this machine where not designed for testing composite laminates. As with most grips, load is introduced on the surface in the form of shear. Shear loading of thick specimen is not considered an adequate technique as early surface delamination can occur, which is not representative of in-field loading and failure scenarios. Therefore a new test fixture has been developed which enables both surface shear and through thickness loading. The Thick Specimen Tensile Loading Fixture (TeST LF) is modular design which allows for variations in coupon thickness and length. The high strength 5160 steel plates and grade 9 cap screws can accommodate loads up to 200kips. A stainless steel rod on each end allows for compensation of small misalignments (Figure 25).

The most effective way to transfer a load through the thickness of a part is to use bolts or pins. Unfortunately, bolted composite joints typically reach at most, 40% of the un-notched strength.[15] Prior research has shown that designing a joint with clamping can increase the joint efficiency up to 100%.[16,17] The TeST LF has been designed to take advantage of this effect. Load transfer is initially applied to the surface of a specimen through friction on the clamping surface. Clamping forces are applied with a predetermined bolt torque. Once friction on the surface can no longer resist the applied load, the TeST LF begins to slip, engaging the bolts. Load is then transferred through the thickness on the bolt hole surfaces.

Figure 25: Thick Specimen Tensile Loading Fixture

ii. Compression Fixture Development

As noted, the Round 1 testing established basic materials properties of thin (4-layer) glass fiber/ epoxy composite coupons containing intentionally manufactured defects.[1] The next component of this work requires manufacture and testing of thicker laminate specimens, potentially up to 20-ply laminates. It is desired to test these specimens in a combined loading fixture (end loaded and side supported) designed in-house and manufactured in a local machine shop.

By applying both a shear load to the clamped, shimmed areas of the specimen and an end load to the terminal ends of the specimen, combined loading fixtures largely mitigate end crushing. According to

ASTM D6641 a compression test of polymer matrix composite material is unsuccessful if end crushing occurs.[7] This fixture for polymer matrix composites does not include side support for the gage section.

Maintaining alignment of the fibers in the 0° direction and preventing fixture misalignment due to complex geometries in the gage section is critical to testing the planned specimens. Implementation of low friction linear bushings will function to help prevent binding even under heavy compressive loads.[3] Binding as a consequence of friction is a primary concern as the alignment system should not carry any of the load for a valid test. Secondary to binding, failure of the housing for the alignment rods was considered for tear-out and failure at the shaft bore as well as stress concentrations at sharp inside corners. The maximum transverse load which could result from specimens with fiber waviness was determined for a 20-layer laminate using Computer Aided Design Environment for Composites (CADEC).[18] Fiber and matrix properties were input and the desired 2% strain level and a maximum transverse stress was calculated by the software. Using the resulting total transverse stress, compressive load on the fixture linear bearings was backed out by modeling each alignment rod as a cantilever beam with a distributed load. The fixture is shown below in Figure 26.

Future work with this fixture will include determination of the ratio of shear loading to end-loading as well as any load the fixture alignment system may be carrying. This will include, but not be limited to, work in characterizing loads transferred by fiber misalignment to the alignment system which could lead to binding. Characterization of the test fixture response will take place prior to testing any specimens for usage in the Effects of Defects program. Due to the significant weight of this fixture, a handling system may also be implemented both to promote safety for technicians and to facilitate expedited testing.

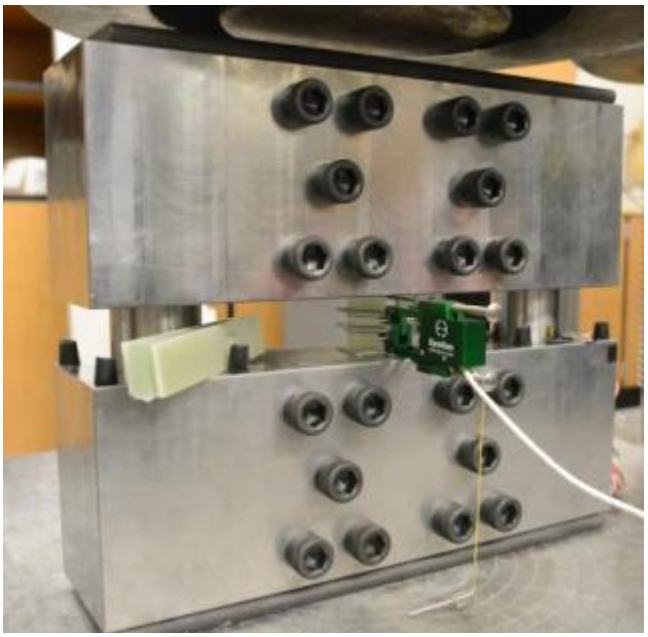

Figure 26: Complete compressive testing assembly with specimen ready for testing.

iii. Initial Thick Laminate Test Results

The first phase of thick laminate testing consists of verifying scaling parameters for control specimen. Initial testing of 8 and 16 ply control laminates in tension and compression have been performed. The purpose of these tests was primarily to evaluate the testing fixtures. The test fixtures performed as expected, that is without complications or unexpected consequences. Preliminary results of the compression test show that bolt torque and shim placement impacts the specimen performance. However, failure stresses are in good agreement with thin laminate compression testing reported on

earlier (-5% deviation). Further tension testing is needed to identify variables in the testing process. Work will continue to improve upon the testing methods in order to ensure that results are repeatable and indicative of actual material response rather than fixture influences.

Once the baseline control scaling parameters have been identified, follow-on tests will examine the effect of porosity, IP and OP waves on uni-axial, 0 -degree fiberglass epoxy laminates as thick as 20 layers. This data is required to validate modeling tools for damage progression on thicker composites. It will also provide information into the scalability of flaws in composites. Due to the success and comprehensive nature of testing on thinner laminates it should not be necessary to test excessive amounts of flaw parameter permutations in order to establish correlation between flaws and mechanical performance. Moreover, it is expected that testing of 8 and 16 ply control specimen will provided insight into scaling that mitigates the need to perform thick laminate testing on multiple layup thicknesses. The following Table details the proposed defect laden test articles.

Table 5: Thick Flawed Laminate Testing Matrix

Flaw Type	Test Type	# of Coupons	Description/Notes
In-Plane	Tension Compression	3 3	Fiber angle 15-30 deg
Porosity	Tension Compression	3 3	5-10% by Volume
Out-Plane	Tension Compression	3 3	Fiber angle 15-30 deg
Total		**18**	

These tests will be considered successful if the following criteria are met: 1) Results of ultimate strength exhibit trends describable through Weibull scaling and/or regression analysis and/or 2) Model prediction of load displacement curves are accurate to within ±5%.

These tests will be considered inconclusive if the following criteria are met: 1) Results of ultimate strength do not exhibit trends describable through Weibull scaling and/or regression analysis and 2) Model prediction of load displacement curves have errors > ±5%.

Should the inconclusive criteria be met, the first recourse will be to adjust material property curves and models. Additionally it may be necessary to perform testing on a larger spectrum of flaw parameters and material thicknesses.

V. Round 2: Analytical Modeling Effort

A. Background

To meet the proposed goals of this project, significant analytical efforts will be continued in a progressive manner through the three rounds. Initial rounds of simple uni-directional coupons have utilized relatively simple material degradation models. These binary models utilize a simple logic that will set certain material properties to zero depending on the type of damage. However, as test specimen become more complex in further rounds, corresponding models will likely need to become more complex. To account for this, two distinct modeling methods have been investigated and will be compared through the entire project: Continuum Damage Modeling (CDM) and Discrete Damage Modeling (DDM). CDM is a "pseudo-representation" that does not model the exact damage but instead updates the constitutive properties as damage occurs. For each individual element:

$$u = \frac{1}{2}\int_V \varepsilon[C]\varepsilon \, dV \tag{1}$$

where:

$$[C] = C(\varepsilon) \tag{2}$$

As the model iterates, the constitutive matrix *C* is updated to reflect equilibrium damage. Whereas DDM actually models the damage as it occurs through the load profile, and is generally thought to be computationally more expensive (Figure 27)[23]. Even though both of these methods have significant advantages and disadvantages, they offer more accurate modeling options than the initial binary method noted above which is a simplified CDM method.

While testing of wind related composite coupons and structures is an integral portion of this research, it will be performed in large part for correlation with analytical data. Several different analytical modeling approaches will be considered, falling into either CDM or DDM categories noted above. In both categories, analytical models will follow a similar path as the testing, from simple coupons toward larger structures, during this research plan. In order to effectively model larger structures, multiscale modeling will be utilized to reduce computational expense as much as possible. This will allow a microscopic model will be utilized in areas of damage while the rest of the structure will utilize a macroscopic model. While both damage modeling techniques will differ over the entire structure, the key differences will be evident in how the damaged area is estimated.

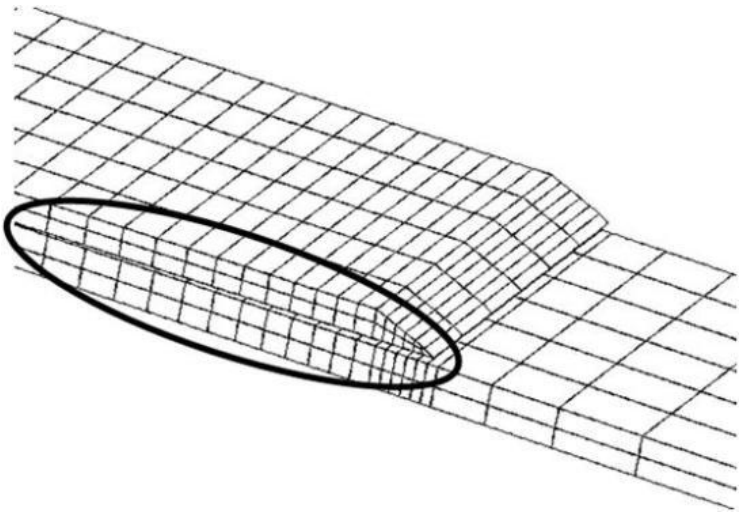

Figure 27: Crack growth (circled) in a stiffener panel visualized utilizing Discrete Damage Model.

i. Continuum Damage Modeling (CDM)

Continuum modeling derives from the assumption that a material is continuous and fills an entire region of space. From this it can be broken into representative volume elements (RVE) such that constitutive equations relate the RVE to the entire structure. However, it is necessary to homogenize the material properties of the RVE which is not always feasible when studying composites.[14] In some instances, the two different materials cannot be represented accurately this way, especially as damage accumulation occurs independently in one of the constituents.

Simple CDM's have been utilized in finite element analysis that account for damage in the fiber and matrix independently. Utilizing a simple material property degradation model, Chang and Chang presented a progressive damage model for laminated composites with a circular hole in tension.[19] Convergence between stress and failure analyses were performed utilizing classical lamination theory considering material nonlinearity and property degradation resulting from damage, respectively. Nonlinear finite element analysis was performed and agreement was found between the analytical and experimental data. In the stress analysis, the equilibrium equation and stress-strain relations were derived. The equilibrium equation took into account that once the laminate was damaged a redistribution of the stresses and strains resulted in degraded material properties. Thus, the equilibrium equation was solved at each step utilizing a Newton-Raphson iteration scheme. The failure criteria were defined based on the failure mechanisms resulting from damage: matrix cracking, fiber-matrix shearing and fiber breakage. Based on these criteria, a property reduction model was implemented reducing certain properties to zero upon failure. Numerical procedures were written based on the following procedural logic:

1. Increase the applied load from P^{n-1} to P^n by a small increment ΔP.
2. Calculate incremental strains Δe_{ij} and incremental stresses $\Delta \sigma_{ij}$ from derived stress-strain relations and equilibrium equations.
3. Update the total stresses σ^n_{ij}.
4. Calculate in-plane stresses in each ply by coordinating transformation.
5. Assess damage using failure criteria equations.
6. Return to the first step if no damage is found or continue to the following steps if damage occurs.
7. Stop, if damage has propagated across the laminate and no more load can be added. Otherwise, continue.
8. Update mechanical properties by applying property degradation model as indicated in Equation 1 above.
9. Redistribute stresses and strains in the laminate by applying equilibrium equations again.
10. Return to step (4).

This logic is also presented as flow diagram (Figure 28) with the damage user-subroutine steps indicated in light blue while standard model routine steps are shown in dark blue. As shown, the subroutine simply performs the failure analysis and then checks for failure. If no failure criteria is met, the load is increased and the model iterates. If a failure criteria is met, then the logic accounts for that damage and checks for ultimate failure. If the ultimate failure criteria is met, then the model stops whereas if it is not, then it iterates by adjusting model inputs as outlined by the damage model that is utilized.

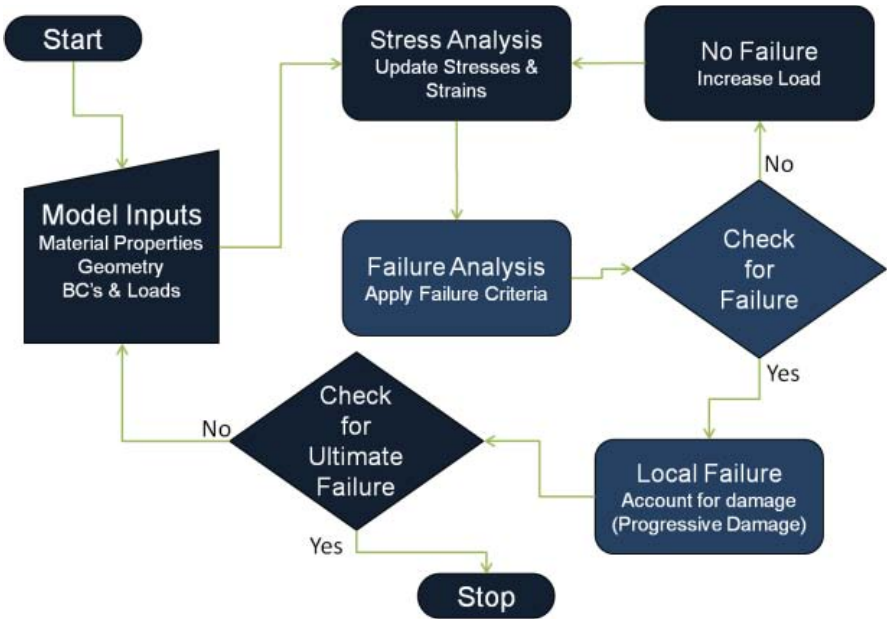

Figure 28: Flow of model and damage progression logic utilized in this research with user-subroutine components shown in lighter blue.

Using this logic, Chang and Chang's results were in agreement between the analytical and experimental data for seven (7) independent laminates. Later, Chang and Lessard performed similar work on damage tolerance of laminated composites in compression with a circular hole.[20] A similar logic as above was utilized resulting in agreement between the analytical and experimental data similar to that noted in the Round 1 Report.

Additional research in this area has been performed by others for many different conditions (e.g. material, matrix, loading, fastening, etc.). Eveil developed a 3D failure analysis methodology for composite laminates.[21] This analysis utilizes a similar logic to Chang above with failure criteria based on Hashin and Yeh. Utilization of this advancement to 3D improved error from 25-30% to as low as 2.6%. Tay et al. have compared material property degradation models, element failure method and strain invariant failure theory.[22] Material property degradation is the method used in each of the papers above. The element failure method modifies nodal forces to reflect damage and is employed with micromechanics based failure criteria. It is suggested that these and other alternative approaches may be superior when translating results from specimen level to component and structural levels.

While these simplified versions show reasonable correlation to experimental data, the accuracy with which they can predict damage beyond initial fiber or matrix failure is dubious. This is largely due to the oversimplified property degradation and failure criteria, though these simplified methods do attempt to account for the constituents independently. Further, these simple models are utilizing a uni-directional material.[23] Hansen, Walker and Donovan presented a multicontinuum technique that keeps each constituent independent and allows for the introduction of additional constituents for more complex materials such as woven fabrics.[24] By utilizing a volume fraction mixture theory, the composite average stress, or strain, may be estimated by summing the stresses, or strains, of each constituent based on the volume ratio of that constituent. By decomposing the average composite stress/strain state into constituent average stress/strain states, a basis is formed from which damage evolution may be predicted at a point of interest. Thus, constituent failure criteria may be based on the constituent average stress which potentially increases the level of accuracy of the model. It must be noted that this multicontinuum technique is the foundation for the Helius:MCT software package available from Firehole Composites (Laramie, WY).

ii. Discrete Damage Modeling (DDM)

Discrete modeling is considered by many to be more consistent with the physical damage of thermosetting polymer reinforced composites. As noted, a continuum approach relies on changing material properties which do not change during damage evolution. Thus, DDM attempts to directly model damage as it would actually occur within a structure as shown in Figure 1 above. It must be noted however, that this method is generally computationally more expensive and is more mesh dependent than CDM.[25] In addition, knowledge *a priori* of the damage location is very helpful as an initial crack may have to be place depending on the type of model.

Several techniques for discrete modeling exist such that crack development and path may be modeled. Originally, discrete models had discrete crack propagation and would be followed by a re-meshing with the new geometry. This cycle is repeated until ultimate failure has been reached based on one of several crack propagation criteria.[26] The discontinuity created by the crack can make re-meshing difficult and extended finite element modeling (XFEM) allows for a crack to propagate without having to re-mesh at each step.

Additionally, the use of cohesive elements has proven a viable option for modeling laminated composites and does not require an initial crack be placed in the model.[27] In summary, a layer of zero thickness cohesive elements with specific traction-separation criteria are placed in areas of interest such as between layers of the laminate. As the traction-separation criterion is met for a specific cohesive element, a separation occurs resulting in crack propagation. Thus, damage evolution is able to modeled discretely. Though, significant time up-front is needed to build meshes as models become very detailed.

B. Improvements from Round 1 CDM Efforts

As noted in the Round 1 report, a simple binary CDM was utilized to initiate damage modeling. The resulting damage from the model was checked and the damage progression compared visually to the test results. It was noted that stress accumulated rapidly in the peak of the wave and increased until fiber-matrix failure and then with each step the damaged area grew. This matches the damage progression noted visually and with a digital image correlation (DIC) system. All Control and IP Wave 1 models were tested in a linear elastic fashion to ensure the boundary conditions and model integrity. The load-displacement results of these models are compared to those from the physical testing with good agreement. Once this agreement was achieved, the damage progression subroutine was turned on and damage was predominantly fiber-matrix and occurred catastrophically at just over 40 kips which reasonably agreed with the physical test data.

Even though these initial modeling efforts showed reasonable agreement, this simple model was found to need improvement to be considered fully functional. To test the full capabilities of this method, the Multi-Angle laminate testing (above) and modeling (below) was implemented to show the limitations and salient features. The modeling effort is continuous through all three rounds working toward better prediction at larger scales. Below is the list of items to aid in finalizing the modeling effort, which allows for stepping toward more complex modeling efforts as listed in Round 1 with a brief update through Round 2.

i. Specific Model Updates through Round 2

Below is the list of items to aid in finalizing the modeling effort, which allows for stepping toward more complex modeling efforts as listed in Round 1 with a brief update through Round 2:

1. **Update and run models for other tested configurations**—Additional modeling of testing configurations will be ongoing through Round 3 to confirm tested configurations of tests performed in all three rounds.
2. **Understand damage type for each model**—Continued review of DIC and other visualization data from each test to ensure consistent damage progression between experimental and analytical analyses. This has been aided by the visualizing the failure type as it occurs in the models (Figure 29).
3. **Compare to strains from model to DIC data and calculated stresses from test data**—An ongoing effort through each round of analytical and experimental correlation (Figure 30).
4. **Modify mesh size and element type to determine sensitivity to each**—Mesh size and element type have shown to have minimal effect on the simple binary CDM. It must be noted that mesh sensitivity and element type will likely have major impacts on the DDM and will continually be tested to ensure optimization.
5. **Test sensitivity to oriented properties**—See Multi-Angle laminate test and model results herein.
6. **Update/add failure criteria and improve strength properties accuracy to improve damage progression subroutine**—As noted below in the Multi-Angle laminate modeling efforts noted below, significant advances are necessary to increase model accuracy. See below for more detail.

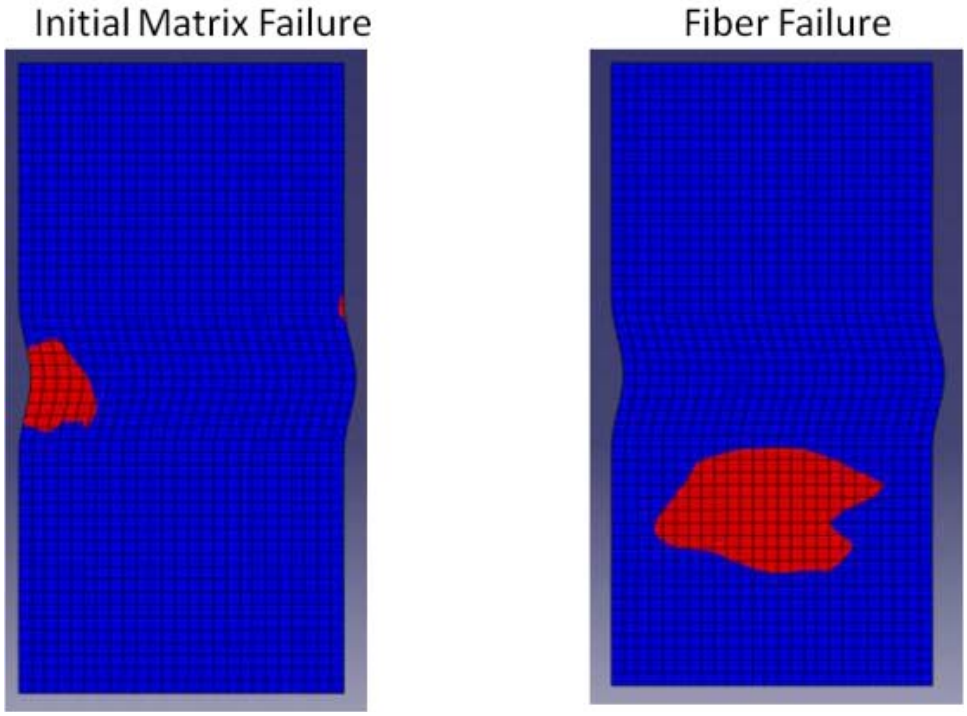

Figure 29: Representative damage type through the damage progression of an IP Wave from the simple binary CDM. This data was then compared with tested specimens and similar damage progression was noted.

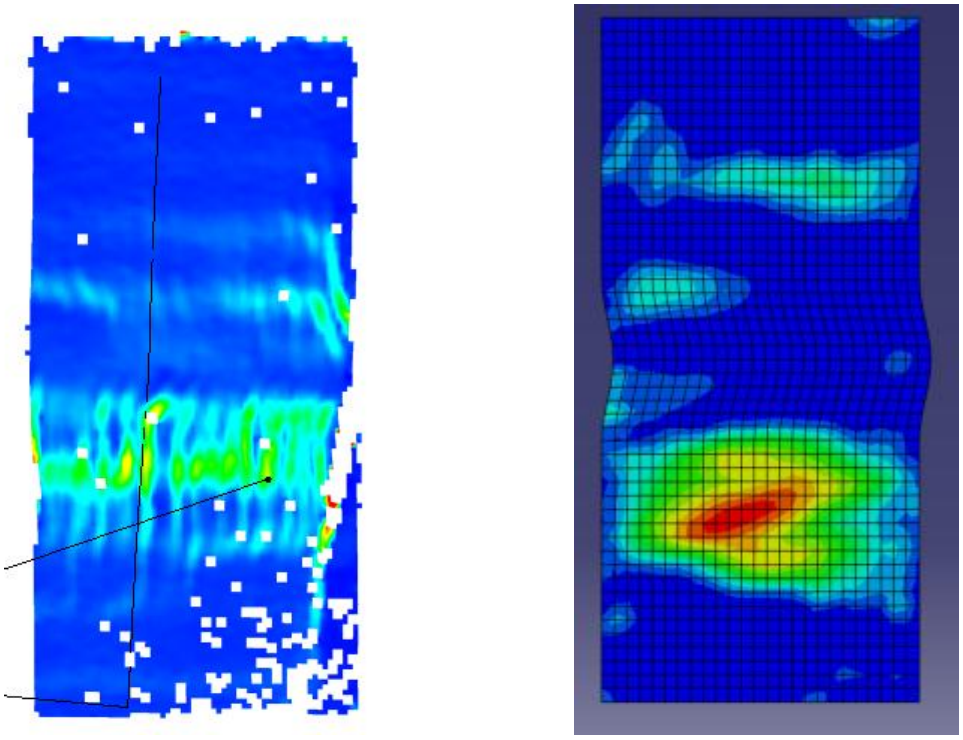

Figure 30: Experimental (left) and analytical (right) comparison of IP Wave coupon in tension.

Further discussion of next steps and advances anticipated in Round 3 may be found in the Future Work section. It is important to note that this modeling has been done with experimental analytical correlations compared to other studies on wind turbine blades which have either modeled the damage progression, or measured the effect of damage without a damage growth model.

C. Multi-Angle Laminate CDM Results & Discussion

Using a similar approach as performed in Round 1, material properties were taken from the test data and put into a linear elastic version of the model. This allowed for confirmation of the properties by superimposing the model data onto the load-displacement curves (Figure 31 & Figure 32). As was apparent in prior instances where this model was used, the model is not able to accommodate for the softening that occurs through the elastic region of the curve in either case. The result is that the model is initially softer before a slightly overestimating before reaching the ultimate load, more so in the tensile case. Ideally, if the model is not able to accurately match the curve, the model would remain conservative and slightly underestimate the stiffness through the entire curve. This would increase confidence that all cases would statistically be represented in the model. Consideration will be paid to this in all future modeling efforts as this is a significant weakness in this simplified model.

Next, the user-subroutine containing the damage logic was implemented and the model was re-run for each tension and compression. Utilization of the test data led to rapid convergence of the model's initial failure point which, as shown in Figure 31 & Figure 32 below, is reasonable though somewhat conservative. Since these curves contain damage growth unlike the initial uni-axial samples, more complete analysis of the experimental/analytical correlation is able to be performed. It is apparent that further modeling work is necessary as the model is not able to match the plateau observed in the either set of test data. To ensure that this was a result of the binary material property degradation model, both the material properties and the failure criteria were modified. While these data are able to confirm the finding that this material property degradation is insufficient, further work with them to ensure an

accurate and repeatable model is needed in Round 3. It is worth noting that these results confirm Task 4 listed above; that further testing of ±45° is not needed. The properties from the Round 1 Control samples were utilized in this testing and the best correlation yet in this study was achieved even with a ±45° layer in the center of the 4-ply laminated.

In summary, the Multi-Angle laminate tensile testing was performed to further prove the capabilities and limitations of the binary material property degradation model. While there is a reasonable convergence of failure point, better approximation of linear elastic region is needed. In addition, the damage growth is misrepresented due to poor material property degradation model and better constitutive property adjustment and failure criteria are needed moving forward.

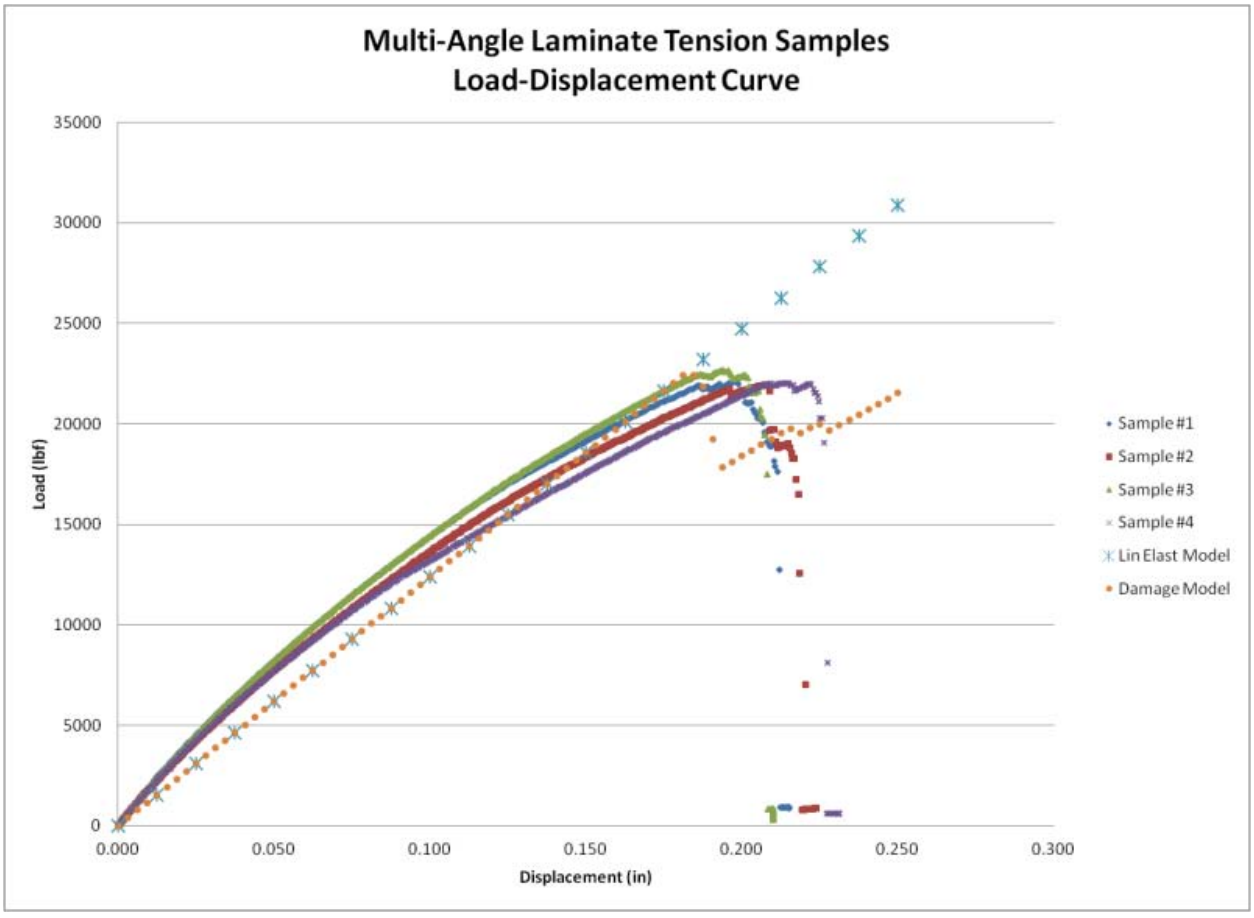

Figure 31: Multi-Angle laminate tensile load-displacement curves with model data superimposed for comparison.

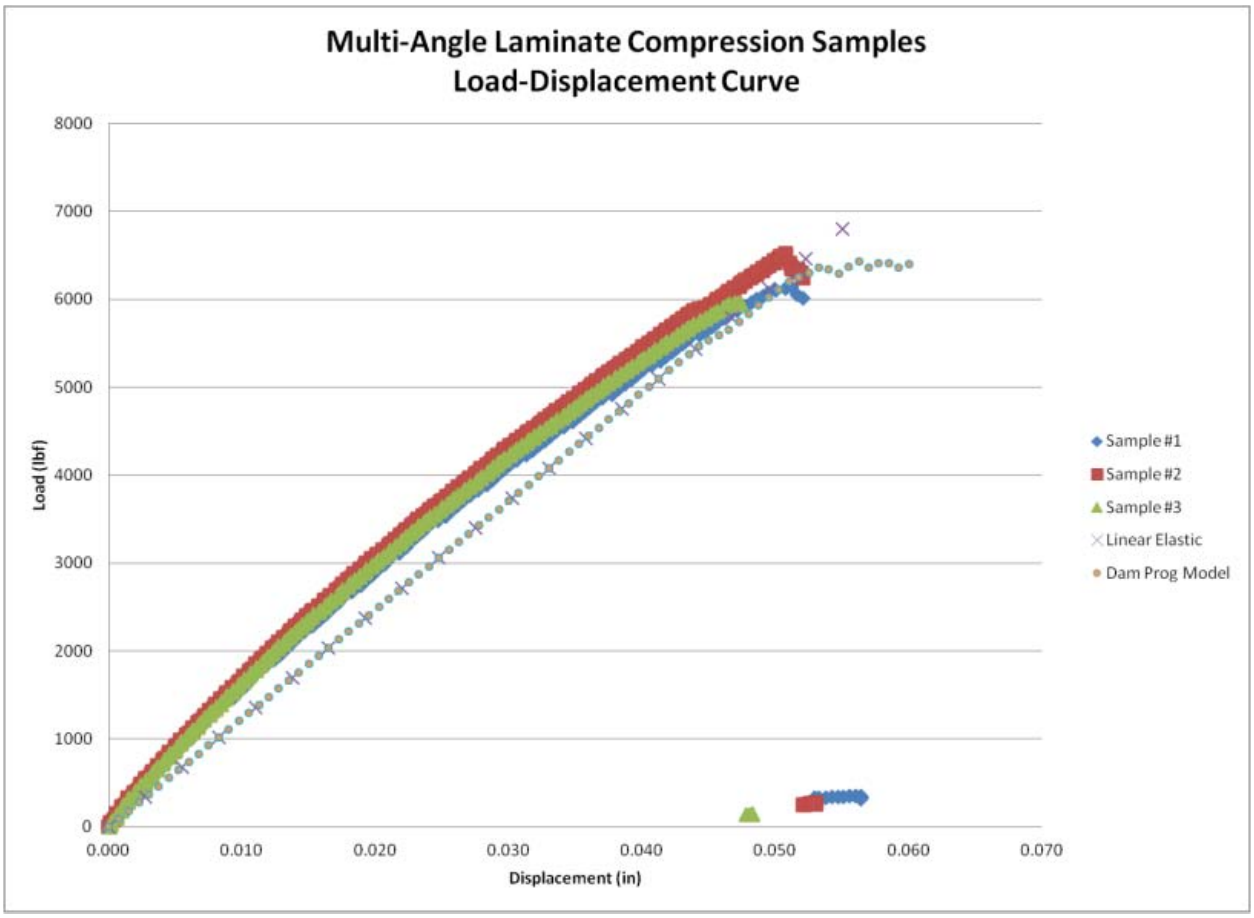

Figure 32: Multi-Angle laminate compression load-displacement curves with model data superimposed for comparison.

D. Initial DDM Efforts

Modeling efforts to utilize discrete damage modeling (DDM) methods were begun in Round 2. Initial models were created by placing layers of cohesive elements between the continuum elements at representative tow thicknesses. To be consistent with the CDM efforts to date, the same IP wave was analyzed. Based on the observed damage progression in all physical testing to date of IP waves, cohesive elements were placed between the fiber tows across the width (Figure 33). In addition, it was deemed acceptable to utilize a 2D model with Abaqus' built in *SHELL SECTION, COMPOSITE tool to calculate through the thickness.[27]

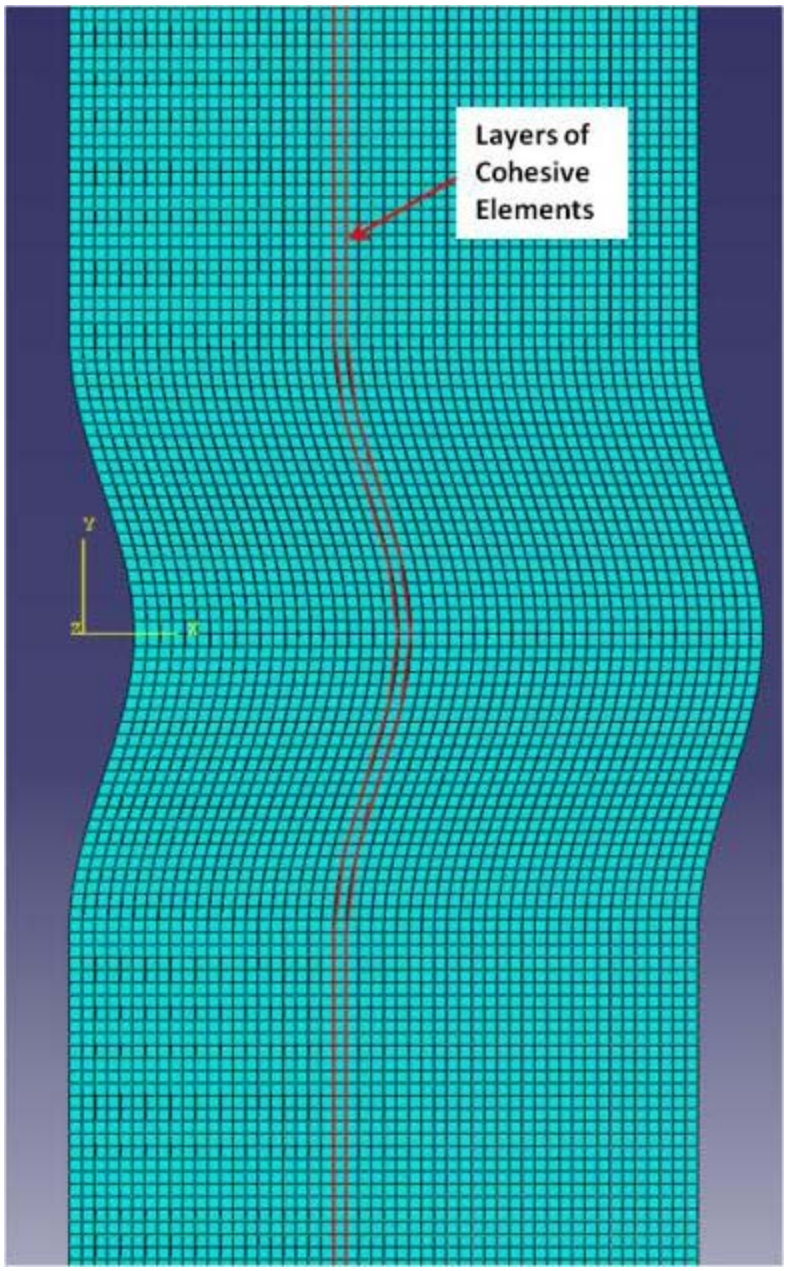

Figure 33: 2D DDM utilizing cohesive elements between each vertical row of continuum elements.

While initial results appear to be promising at the time of the publication of this report, further work and analysis is needed before correlation can be compared. Largely material properties estimated for the cohesive elements need to be verified. Physical testing for transverse properties of these materials has not been directly performed. Initial calculations appear to be lacking and either additional physical testing or research to determine a robust method of estimating these properties must be performed. However, as noted below in Figure 34, this method does show initial promise as the cohesive elements are failing in the same location as noted visually and in DIC imagery. In short, cracking has been observed in the area where the wave begins and as noted in Figure 34 damage has occurred between the fiber tows. Gaps are observed between the tows. Sliding is also observed as the elements are shifting different amounts noted by the changes in shape. While further work is needed, these preliminary results are promising and suggest that this method will continue to be of interest.

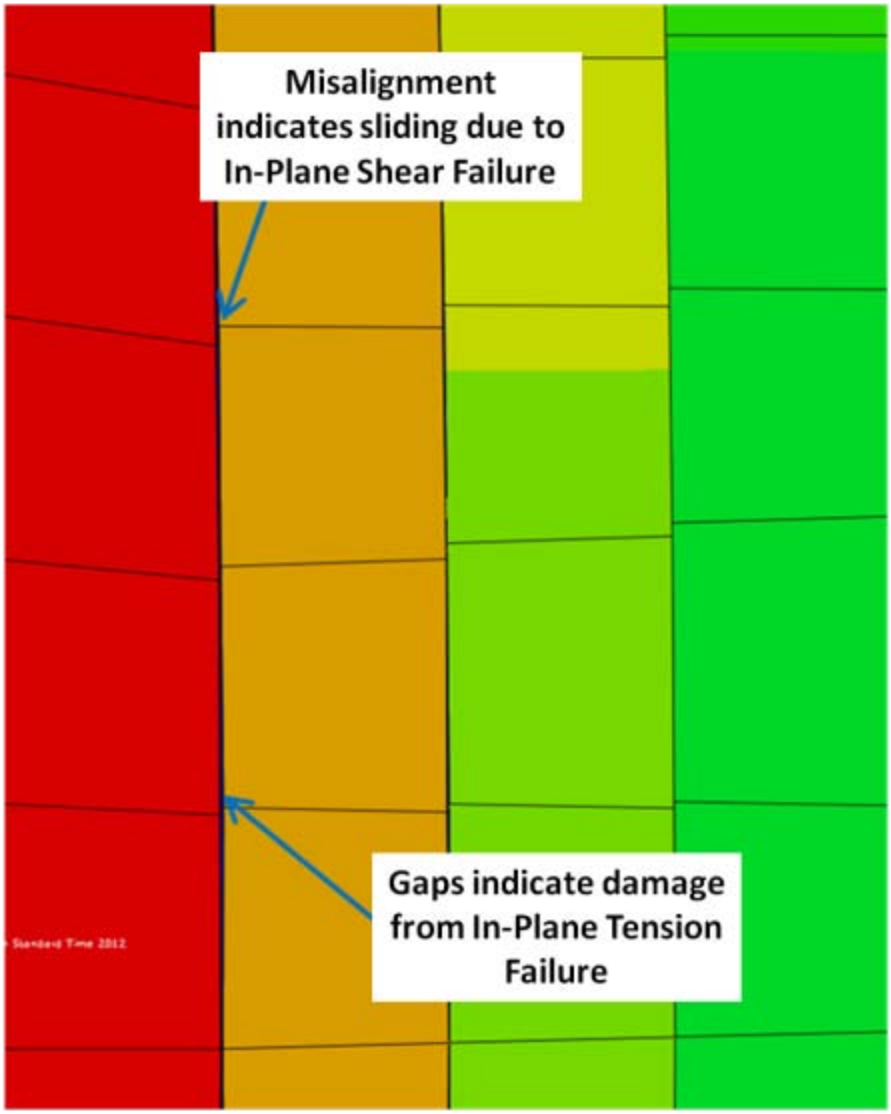

Figure 34: Close-up of failure between the fiber tows indicating that cohesive elements initially fail in the same location as noted visually and in DIC imagery.

Note that Figure 34 is the discrete damage modeling equivalent of Figure 31 & Figure 32 which utilized a continuum approach. A similar discrete approach for damage progression will be investigated for both OP waves and porosity. Since initial failures in OP Wave samples have been noted to be through the thickness or interlaminar, the approach toward modeling change. It will likely necessitate a move to 3D models with cohesive elements placed not only through the thickness (Figure 35).

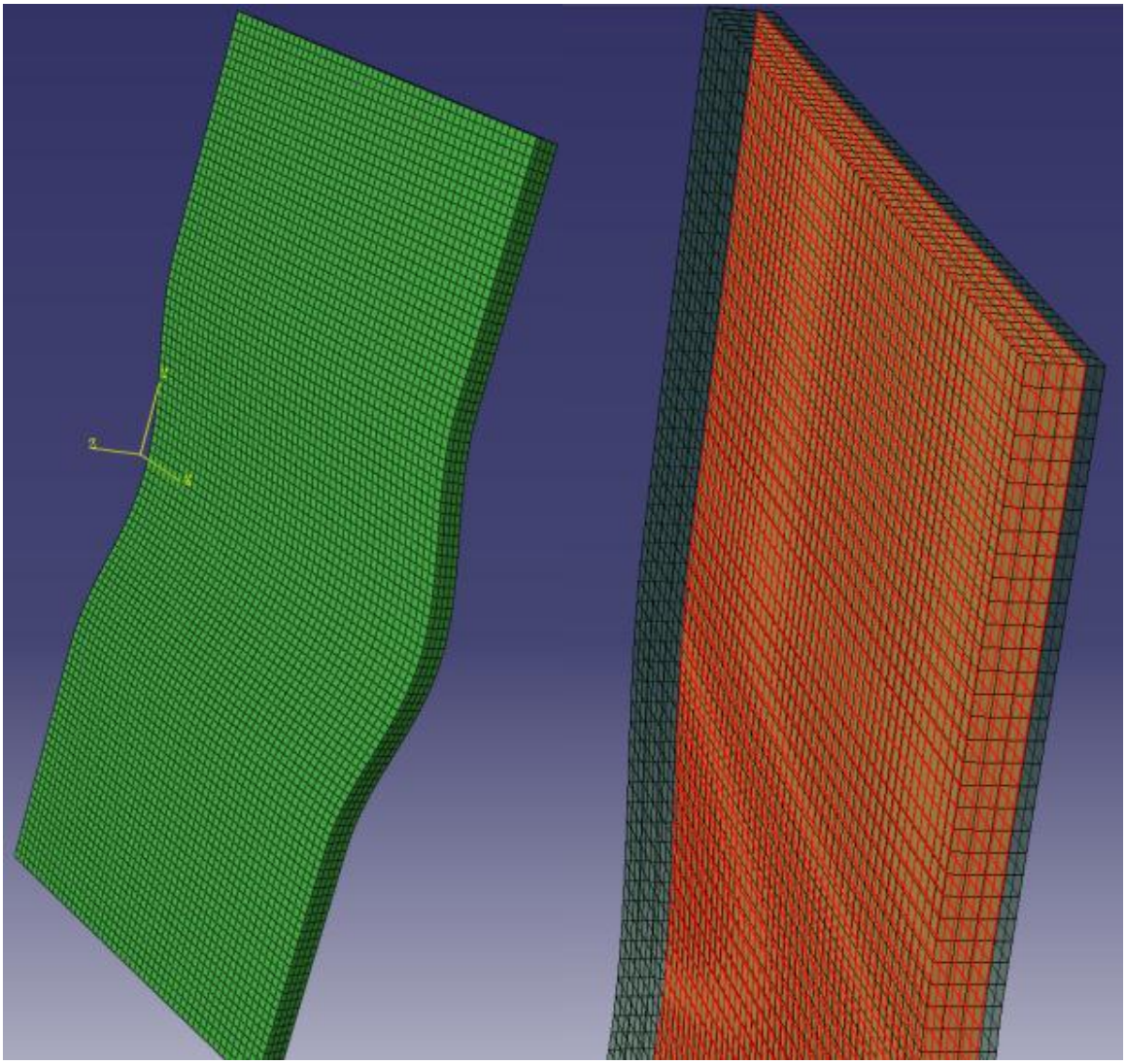

Figure 35: An IP Wave in a 4-ply 3D model (left) with cohesive elements between each ply layer as highlighted on the right.

VI. Conclusions

The work presented herein indicates that not only have the results of Round 1 been built upon, but that steps have been made along several fronts in Round 2. These steps have resulted in broader data ranges and met the goal of moving toward larger scale testing and modeling. Further steps in these directions will be continued in Round 3 as outlined in the Future Work section found below.

A significant effort has been given to improving the flaw laminate manufacturing techniques. Data from the thin laminate testing has shown that these more consistent manufacturing processes have improved the range, and in some cases the consistency, of the test data. In particular, the new OP wave specimens showed failure modes more representative of what one would expect to see in the field. Additionally, the porosity introduction technique achieved much higher levels porosity in the test articles and preliminary results from a new method used to characterize porosity content using radiodensity shows promise. All thin laminate flawed specimen tests showed appropriate mechanical responses and repeatable results successfully building upon the results from Round 1. This coupled with the comprehensive nature of the testing has enabled the generation of database for which high levels of confidence exists. It is expected that thick laminate testing will reveal that these results can be scaled to larger and more complicated structures. In addition, Multi-Angle and Delamination testing were successfully performed for flaw free laminates. Results correlate well with previous data and provided load and material property data necessary for improved analytical/experimental correlations.

Thick laminate control testing has begun and the results look promising. Samples tested in compression show results on par with expectations. In order to minimize fixturing effects, some minor variable such as bolt torque, shim material and spacing have been isolated for further investigation. First efforts with the tension fixture showed complications due to tear out as expected. Further tests will evaluate the laminate pin strength, clamp load friction, bolt placement and variations to the layup schedule of test articles. It is expected that the tear out issue will be resolved quickly by evaluating these results coupled with characteristic length analysis.[28]

Finally, progress has been achieved in modeling efforts through Round 2. Both CDM and DDM approaches have shown promise to model damage progression. In particular, CDM approaches have been utilized more than DDM and a variety of improvements have been made through Round 2. These include several steps, outlined above, to that have successfully improved correlation to test and DIC data. Also, proving the initial binary material property degradation model utilizing the Multi-Angle Laminate test results was deemed critical from the Round 1 efforts. While reasonable correlation was achieved through the elastic region, mechanical responses after initial damage onset were not accurate. This has led to the conclusion that the binary material property degradation model is insufficient and must be improved. DDM work has progressed utilizing cohesive elements in areas where failure is anticipated. While additional work to ensure correct properties is necessary, the concept appears to be working. Overall, both methods have shown promise and will continue to fine tuned through Round 3 to improve analytical/experimental correlation. Additional details of this work may be found in References 29 and 30.

VII. Future Work

While significant progress has been noted above, there is still substantial work to complete this study. Parallel work will continue on both Flaw Characterization and Effects of Defects to achieve these goals. The steps for each are outlined below will be the basis for the Round 3 portion of this study.

1. Flaw Characterization & Defect Risk Management

a. Flaw Data Acquisition
   i. Review, evaluate and report on repair work orders from Sandia Reliability Database. Attempt to establish new partnerships with industry
   ii. Collect data more on as-built flawed blades from NREL with the use of NDE
b. Compile collected flaw data into a succinct database/summary
c. Continued evaluations of NDI technologies
   i. Review of Sandia technology round robin results
   ii. Quantify probability of detection for use in Defect Risk Management studies
d. Characterization of critical defects
   i. Continued testing of laminates increasing in scale
   ii. Finalize criticality evaluation metric
e. Development of Reliability Protocols for Defect Risk Management
   i. Identify parameters from Effects of Defects Damage Progression Modeling
   ii. Finalize Criticality/Severity metrics and input data
   iii. Develop probabilistic evaluation tools
      a. Performed on an as-built defect laden part utilizing characterization information, statistics on flaw distributions and the probability of defect detection
      b. Develop limit state function(s)
      c. Evaluate and select a probabilistic reliability modeling method. Methods under investigation: Expert Systems, First Order Reliability Method, β-Method, Response Surface Method & Taguchi Methods
f. Report on indices to serve as a guide for acceptable values in future reliability assessments
g. Monitor any programs which might utilize the procedures developed herein
h. Continue to complement on-going activities of entire BRC and work in conjunction where possible

2. Effects of Defects: Round 3 Analytical Modeling

a. Improve user-subroutine of CDM approach.
   i. Implement degrading properties instead of zeroing properties upon damage onset.
   ii. Improve/modify failure criteria.
   iii. Improve models ability through damage progression.
   iv. Investigate/utilize Abaqus/Explicit to improve damage progression modeling.
   v. Modify to analyze 3D mesh.
b. Begin DDM utilizing 3D mesh.
   i. Add cohesive elements.
   ii. Substructure by beginning to integrate superelements or similar approach.
c. Utilize both CDM and DDM models to predict and correlate to Round 2 physical testing for all three flaw types.
d. Generate 3D mesh utilizing accurate CAD of defects.
e. Increase scale.
   i. Investigate and use superelements to aid in substructuring if applicable.
f. Correlate to larger scale testing.
g. Identify strengths and weaknesses of CDM and DDM and compare results of these modeling methods.

References

[1] Riddle, TW, Nelson, JW and Cairns DS. *EFFECTS OF DEFECTS IN COMPOSITE WIND TURBINE BLADE: Round 1,*SANDIA Report: SAND2011-8110, Sandia National Laboratory, Albuquerque, NM, June 2011.

[2] SANDIA Blade Reliability Collaborative Meeting Conversation, August 2010, Albuqueque, NM.

[3] Shapurian, T., Damoulis, P. D., Reiser, G. M., Griffin, T. J., Rand, W. M., "*Quantitative evaluation of bone density using the Hounsfield index*," The international journal of oral and maxillofacial implants, Vol. 21, 2006, No. 2, pp. 290-298.

[4] Email correspondence from Steve Nolet, Principal Engineer & Director of Innovation of TPI Composites, Warren, RI.

[5] ASTM D3039. *Standard test method for tensile properties of polymer matrix composite materials*.

[6] ASTM D3410. *Standard Test Method for Compressive Properties of Unidirectional or Cross-ply Fiber Resin Composites, American Society for Testing and Materials*.

[7]ASTM D6641. *Standard Test Method for Compressive Properties of Polymer Matrix Composite Materials Using a Combined Loading Compression (CLC) Test Fixture.*

[8] ASTM D5528. *Standard Test Method for Mode I Interlaminar Fracture Toughness of Unidirectional Fiber-Reinforced Polymer Matrix Composite.*

[9] Mandell, J. F., & Samborsky, D. D. (1997). *DOE/MSU composite material fatigue database: test methods, materials, and analysis.*

[10] Nielsen, L. E. J Appl Polym Sci 1966, 10, 97–102.

[11] Nielsen, L. J Comp Mater 1967, 1, 100–119.

[12] Nielsen, L. E.; Landel, R. F. Mechanical Properties of Polymers and Composites; Marcel Dekker: New York, 1994; Chapter 7

[13] TPI-RI Materials Testing Lab, "Cmpressive Testing of Specimens with Artifically High Void Content", Doc.No.:10022, 2010

[14] M. R. Wisnom, "Size effects of fibre-composite materials," Composites Science and Technology, vol. 59, 1999.

[15] L. J. Hart-Smith, "Theory & Analysis for Optimization of composite Multi-Row Bolted Joints," in ACEE Composite Structures Technology Conference, 1984.

[16] J. STOCKDALE and F. MA TTHEWS, "The effect of clamping pressure on bolt bearing loads in glass fibre-reinforced plastics," Composites, vol. Jan, 1979.

[17] J. Crews, "Bolt-Bearing Fatigue of a Graphite/Epoxy Laminate," NASA TM81851, 1980.

[18] Barbero, E. J. (1999). Introduction to composite materials design; and companion CADEC software package: http://www.mae.wvu.edu/barbero/cadec.html, CRC Press; 2nd edition, 2011.

[19] Chang, F. K. & Chang, K. Y. (1987) A Progressive Damage Model for Laminated Composites Containing Stress Concentrations. *Journal of Composite Materials*, v21, 834-855.

[20] Chang, F. K., & Lessard, L. B. (1991). Damage tolerance of laminated composites containing an open hole and subjected to compressive loadings. I: Analysis. *Journal of Composite Materials, 25*, 2-43.

[21] Evcil, A. (2008) Simulation of Three Dimensional Progressive Damage in Composite Laminates. *Intl Journal of Mechanics*, v2, 67-75.

[22] Tay, T. E., Tan, V. B. C., & Tan S. H. N. (2005). Method for Progressive Damage in Composite Structures. *Journal of composite Materials*, *39*, 1659-1675.

[23] Garnich, M.R. and Hansen, A.C. (1997). A Multicontinuum Theory for Thermal-Elastic Finite Element Analysis of Composite Materials, *Journal of Composite Materials*, 31(1): 71–86.

[24] Hansen, AC; Walker, JL; and, Donovan, RP (1994). A finite element formulation for composite structures based on a volume fraction mixture theory. *Intl Journal of Engineering Science*, 32(1), 1-17.

[25] Breitzman, T; Iarve, E; Lipton, R; Mollenhauer, D; and, Zhou, E (2010). Multiscale discrete damage modeling in laminated composites. *ECCM 2010: IV European Conference on Computational Mechanics*.

[26] P.O. Bouchard, F. Bay, Y. Chastel, I. Tovena (2000). Crack propagation modeling using an advanced remeshing technique**.***Comput. Methods Appl. Mech. Engrg.*, 189, pp. 723–742.

[27] Abaqus Reference Manual, Simulia, Providence, RI.

[28] Whitney, J. and Nuismer, R. "Stress Fracture Criteria for Laminated Composites Containing Stress Concentrations" *Journal of Composites Materials*, 1974.

[29] Riddle, T.W., Cairns D.S. & Nelson, J.W. (2011). Characterization of Manufacturing Defects Common to Composite Wind Turbine Blades: Flaw Characterization. *AIAA SDM Conference Denver*; April 2011.

[30] Nelson, J.W., Cairns D.S., &Riddle, T.W. (2011). Characterization of Manufacturing Defects Common to Composite Wind Turbine Blades: Effects of Defects. *AIAA SDM Conference Denver*; April 2011.

Appendix

A. Round 2 Thin Laminate Testing Raw Results.

Table 6: Results from Round 2 Compression and Tension testing of IP Wave Samples.

In-Plane Waves		Average	Peak load		Peak stress		Strain at	Modulus of Elasticity	
Test type	Sample name	Angle	kips	kN	ksi	Mpa	Failure	Msi	Gpa
Compression	C-IPA-1-2183	17	-7.07	-31.4	48.0	331	0.70%	2.38	16.4
	C-IPA-2-2183	11	-7.03	-31.3	48.9	337	0.54%	2.00	13.8
	C-IPA-3-2183	16	-7.05	-31.4	46.4	320	0.58%	2.59	17.9
	C-IPA-4-2183	16	-7.10	-31.6	48.9	337	1.01%	4.84	33.4
	C-IPA-5-2183	15	-7.17	-31.9	49.4	341	0.86%	0.84	5.77
	C-IPB-1-2173	21	-6.03	-26.8	40.6	280	0.80%	2.41	16.6
	C-IPB-1-2181	27	-4.93	-21.9	34.6	238	0.90%	1.88	13.0
	C-IPB-2-2173	21	-5.56	-24.7	38.1	262	0.81%	1.23	8.50
	C-IPB-2-2181	27	-4.94	-22.0	34.4	237	0.90%	1.23	8.49
	C-IPB-3-2181	26	-5.31	-23.6	37.2	256	0.92%	1.28	8.83
	C-IPB-4-2181	29	-4.97	-22.1	32.8	226	0.85%	1.40	9.63
	C_IP_1_2195	18	-5.48	-24.4	39.1	269	0.90%	0.89	6.12
	C_IP_2_2195	20	-5.85	-26.0	37.9	261	0.80%	1.01	6.95
	C_IP_3_2195	19	-6.20	-27.6	38.5	265	0.90%	0.99	6.84
Tension	T_IPA_1_2173	17	18.6	82.5	64.8	447	3.26%	3.41	23.5
	T_IPA_1_2183	12	21.6	95.9	75.2	519	3.40%	3.03	20.9
	T_IPA_2_2173	21	18.0	80.2	63.7	439	2.85%	3.02	20.8
	T_IPA_2_2183	14	25.3	112.6	85.9	592	4.07%	2.98	20.6
	T_IPA_3_2183	16	23.8	105.9	81.7	563	3.69%	3.04	21.0
	T_IPA_4_2183	16	23.5	104.4	82.1	566	3.64%	3.08	21.2
	T_IPA_5_2184	16	22.7	101.0	79.4	548	3.87%	2.95	20.4
	T_IPB_1_2181	30	8.67	38.6	15.0	103	2.71%	1.10	7.61
	T_IPB_2_2181	36	8.68	38.6	14.9	103	2.85%	1.02	7.05
	T_IP_1_2195	17	20.61	91.7	65.8	454	3.10%	2.98	20.5
	T_IP_2_2195	16	21.58	96.0	69.5	479	3.40%	2.81	19.4
	T_IP_3_2195	11	21.27	94.6	74.0	510	3.20%	3.04	21.0

Table 7: Results from Round 2 Tension testing of OP Wave Samples.

Out-Of-Plane Waves		Fiber	Peak load		Peak stress		Strain at	Modulus of Elasticity	
Test Type	Sample name	Angle	kips	kN	ksi	Mpa	Failure	Msi	Gpa
Tension	T_OPA_1_2179	6	30.9	137.5	108.6	749	5.00%	3.12	21.5
	T_OPA_2_2179	6	32.8	145.7	116.0	800	5.16%	3.13	21.6
	T_OPA-1-2168	6	30.1	133.9	107.2	739	4.76%	3.17	21.9
	T_OPB_1_2168	8	29.1	129.3	102.9	710	4.63%	2.99	20.6
	T_OPB_2_2168	9	26.5	117.7	94.8	654	4.09%	2.99	20.6
	T_OP_C_2_2197	25	26.9	119.6	94.1	649	4.80%	1.92	13.2
	T_OP_D_1_2196	23	21.6	95.9	78.5	542	4.20%	2.00	13.8
	T_OP_D_2_2196	25	23.7	105.3	85.2	587	4.30%	2.05	14.1
	T_OP_E_1_2197	25	28.2	125.6	100.2	691	5.30%	1.55	10.7
	T_OP_E_2_2197	26	22.4	99.5	80.1	552	4.60%	1.60	11.0
	T_OP_G_1_2196	4	34.8	154.7	127.5	879	5.50%	3.37	23.2
	T_OP_G_2_2196	6	35.1	156.2	127.5	879	5.90%	3.25	22.4
	T_OP_G_3_2196	6	34.2	152.1	123.8	854	5.30%	3.38	23.3

Table 8: Results from Round 2 Compression and Tension testing of Porosity Samples.

Porosity		% by	Peak load		Peak stress		Strain at	Modulus of Elasticity	
Test Type	Sample name	Matrix	kips	kN	ksi	Mpa	Failure	Msi	Gpa
Compression	C_P_1_2148	14	-8.0	-35.6	52.8	364	0.69%	0.73	5.04
	C_P_1_2184	8	-11.8	-52.6	75.6	521	0.95%	5.23	36.1
	C_P_1_2185	9	-11.4	-50.8	73.5	507	0.90%	1.96	13.5
	C_P_2_2148	13	-10.4	-46.3	70.6	487	1.24%	5.98	41.2
	C_P_2_2184	8	-11.1	-49.2	73.9	509	1.52%	5.29	36.5
	C_P_3_2148	8	-10.6	-46.9	71.7	494	1.40%	5.45	37.6
	C_P_3_2184	9	-10.0	-44.5	65.6	453	1.13%	5.95	41.0
	C_P_4_2184	11	-10.9	-48.7	73.2	505	1.48%	5.33	36.7
	C_P_4_2185	7	-11.3	-50.2	73.0	503	1.44%	5.51	38.0
	C_P_5_2185	9	-11.5	-51.0	72.9	503	1.39%	5.70	39.3
Tension	T_P_1_2151	1	38.2	170.1	134.8	929	6.35%	3.29	22.7
	T_P_1_2167	3	36.0	160.1	121.8	840	6.00%	3.14	21.6
	T_P_1_2184	5	38.9	173.0	128.6	887	6.32%	3.13	21.6
	T_P_1_2185	8	40.4	179.8	128.8	888	6.61%	3.03	20.9
	T_P_2_2148	7	37.0	164.7	128.9	889	5.98%	3.22	22.2
	T_P_2_2149	1	38.6	171.7	133.5	921	6.42%	3.22	22.2
	T_P_2_2184	6	40.4	179.8	135.1	932	6.71%	3.13	21.6
	T_P_3_2184	5	37.8	168.2	124.2	857	5.83%	3.17	21.9
	T_P_4_2185	6	37.9	168.4	119.7	825	6.62%	2.82	19.5
	T_P_5_2185	11	35.8	159.0	114.5	790	5.89%	2.94	20.2
	T_P_1_2146	<1	36.5	162.3	122.0	841	6.10%	3.02	20.8
	T_P_2_2146	<1	34.6	153.7	114.7	791	6.20%	2.93	20.2
	T_P_2_2151	<1	36.8	163.9	126.6	873	5.89%	3.24	22.3

B. Round 2 Thin Laminate Load-Displacement and Stress-Strain Curves.

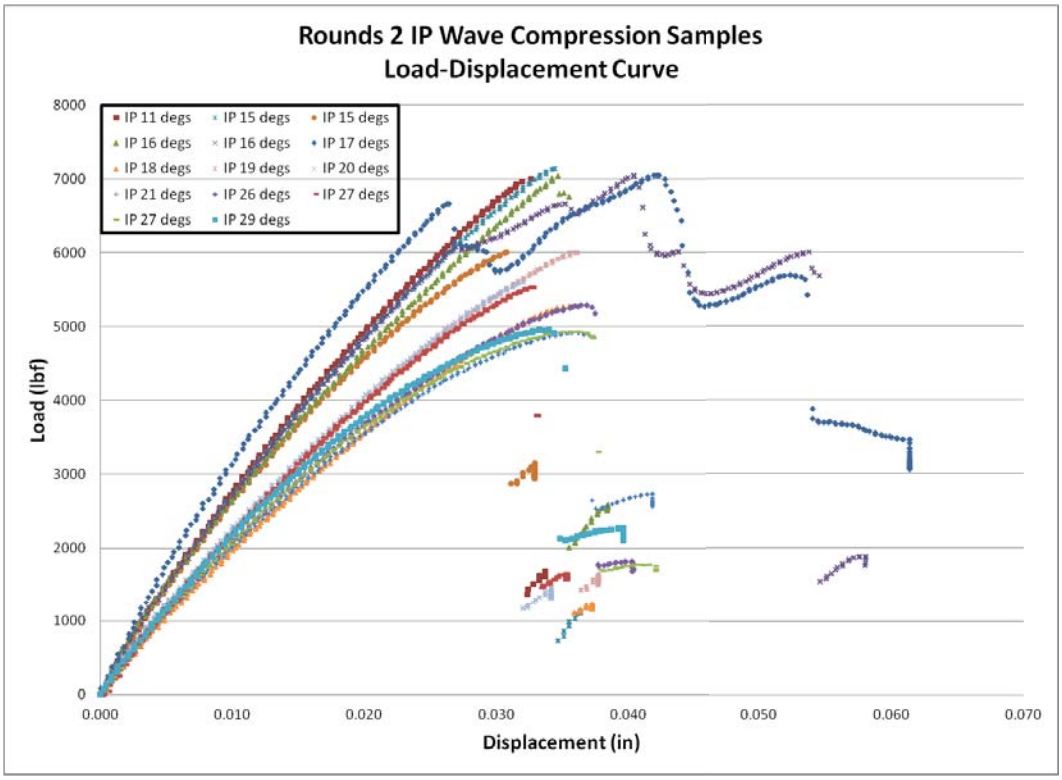

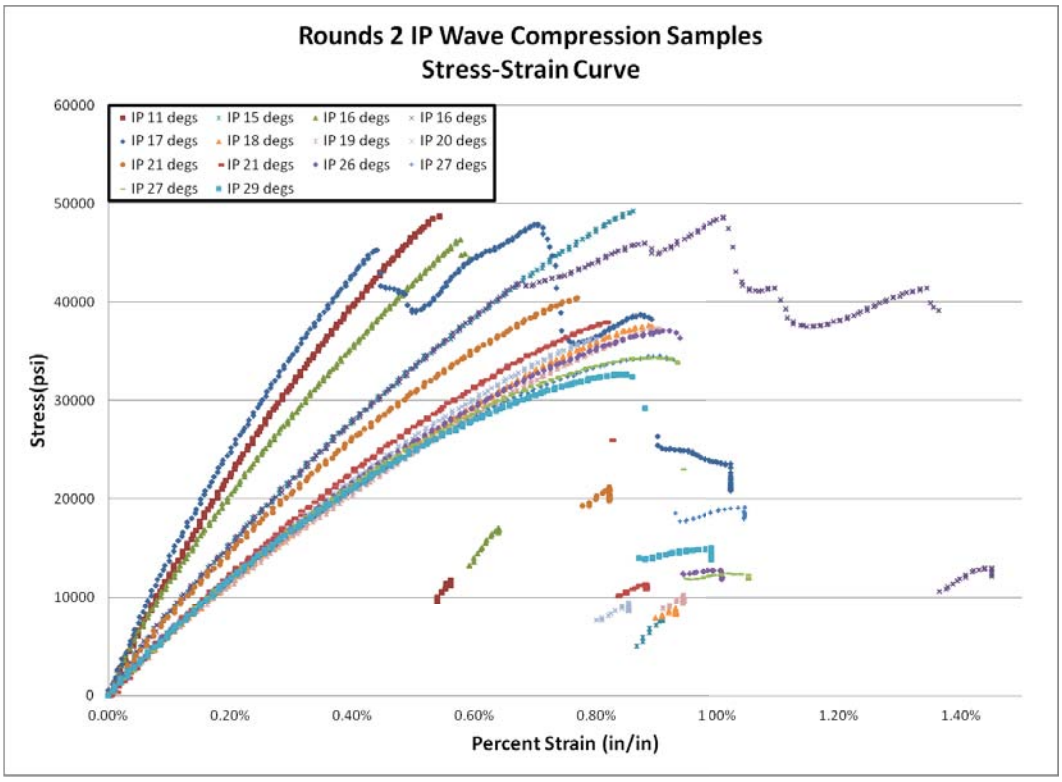

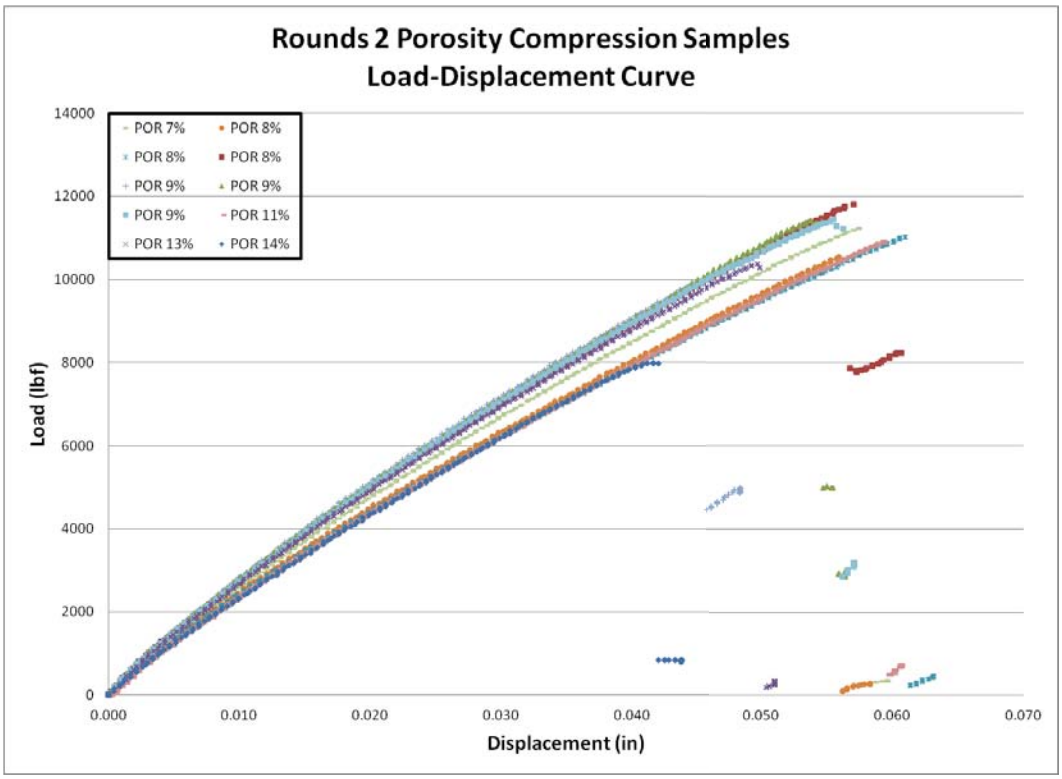
Rounds 2 Porosity Compression Samples
Load-Displacement Curve
POR 7%
POR 8%
POR 8%
POR 8%
POR 9%
POR 9%
POR 9%
POR 11%
POR 13%
POR 14%
Load (lbf)
14000
12000
10000
8000
6000
4000
2000
0
0.000
0.010
0.020
0.030
0.040
0.050
0.060
0.070
Displacement (in)

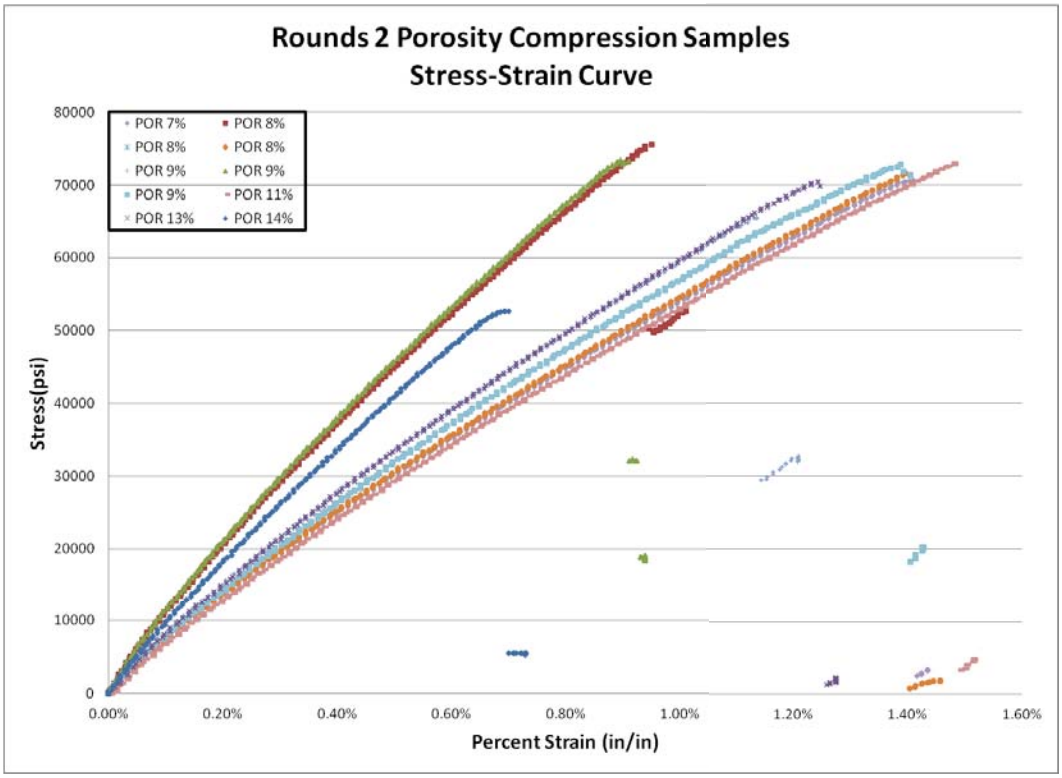
Rounds 2 Porosity Compression Samples
Stress-Strain Curve
POR 7%
POR 8%
POR 8%
POR 8%
POR 9%
POR 9%
POR 9%
POR 11%
POR 13%
POR 14%
Stress(psi)
80000
70000
60000
50000
40000
30000
20000
10000
0
0.00%
0.20%
0.40%
0.60%
0.80%
1.00%
1.20%
1.40%
1.60%
Percent Strain (in/in)

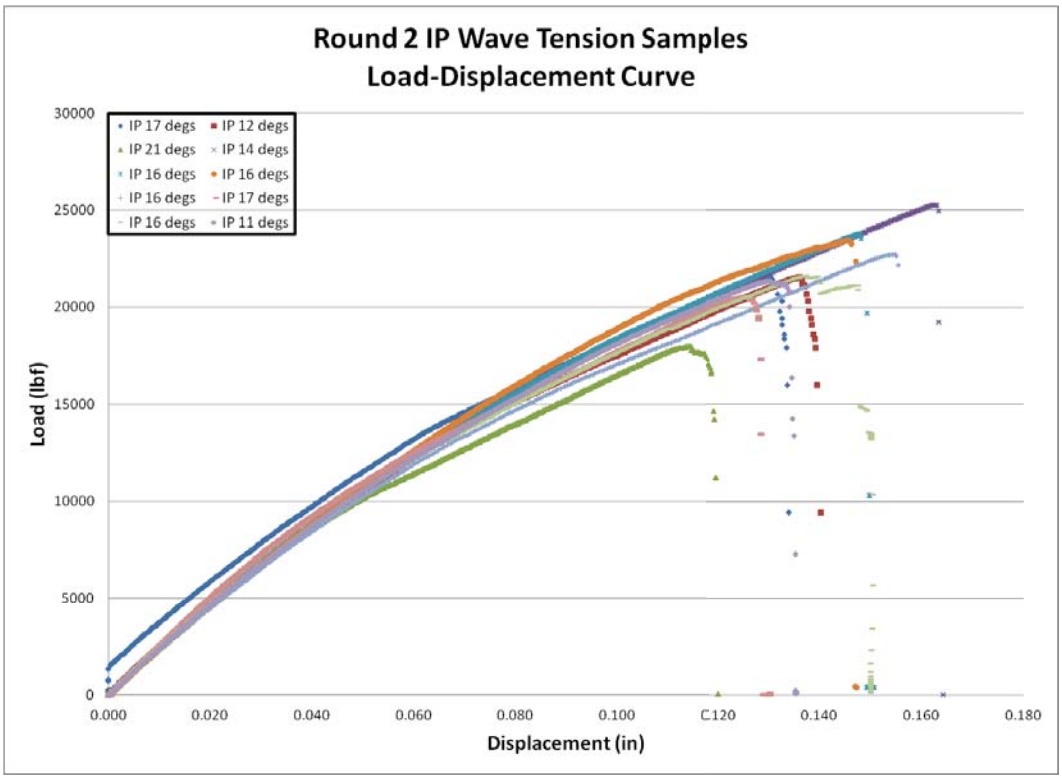
Round 2 IP Wave Tension Samples
Load-Displacement Curve
IP 17 degs
IP 12 degs
IP 21 degs
IP 14 degs
IP 16 degs
IP 16 degs
IP 16 degs
IP 17 degs
IP 16 degs
IP 11 degs
Load (lbf)
30000
25000
20000
15000
10000
5000
0
0.000
0.020
0.040
0.060
0.080
0.100
0.120
0.140
0.160
0.180
Displacement (in)

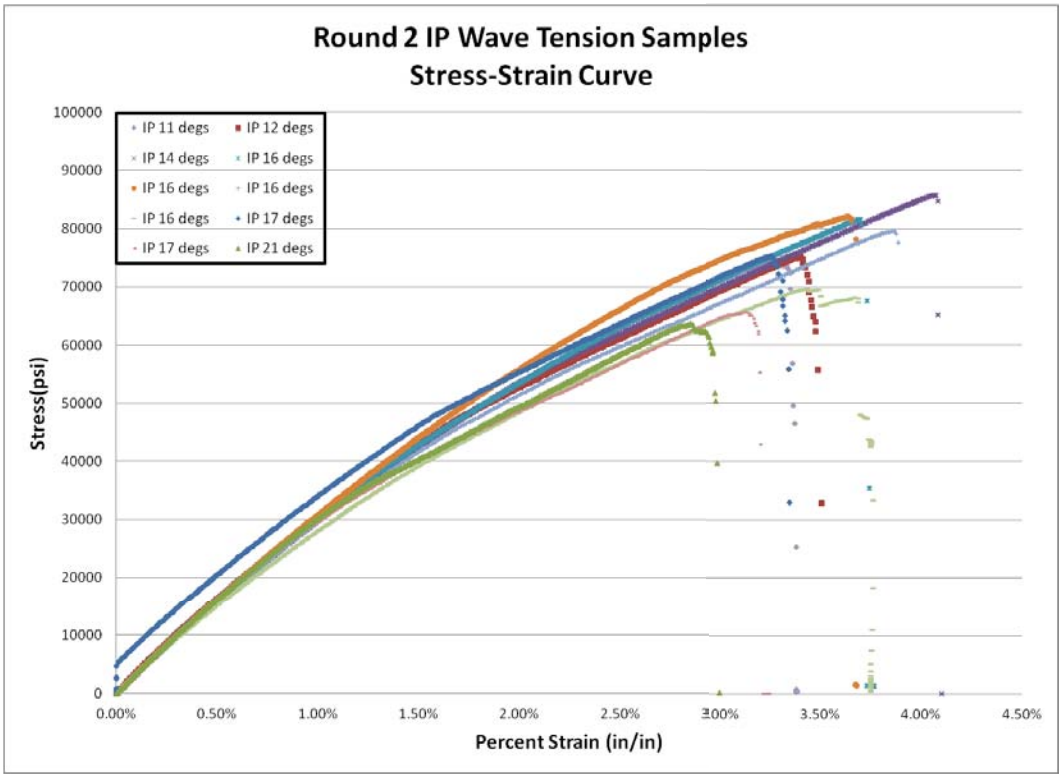
Round 2 IP Wave Tension Samples
Stress-Strain Curve
IP 11 degs
IP 12 degs
IP 14 degs
IP 16 degs
IP 16 degs
IP 16 degs
IP 16 degs
IP 17 degs
IP 17 degs
IP 21 degs
Stress(psi)
100000
90000
80000
70000
60000
50000
40000
30000
20000
10000
0
0.00%
0.50%
1.00%
1.50%
2.00%
2.50%
3.00%
3.50%
4.00%
4.50%
Percent Strain (in/in)

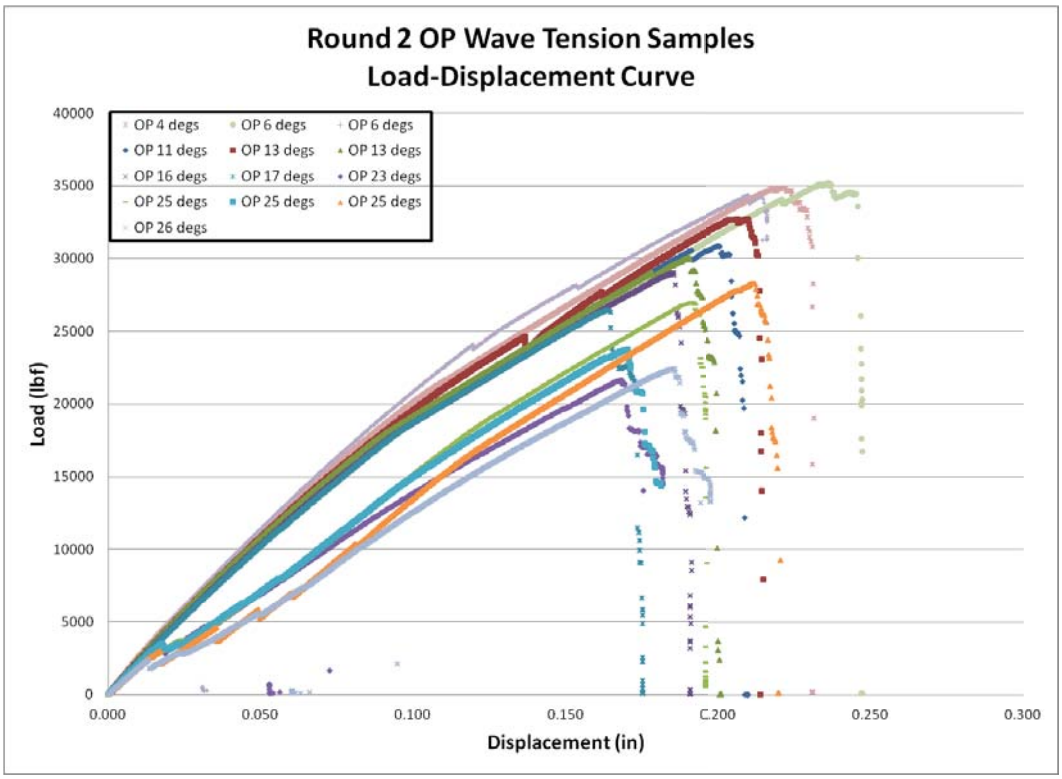
Round 2 OP Wave Tension Samples
Load-Displacement Curve
OP 4 degs
OP 6 degs
OP 6 degs
OP 11 degs
OP 13 degs
OP 13 degs
OP 16 degs
OP 17 degs
OP 23 degs
OP 25 degs
OP 25 degs
OP 25 degs
OP 26 degs
Load (lbf)
40000
35000
30000
25000
20000
15000
10000
5000
0
0.000
0.050
0.100
0.150
0.200
0.250
0.300
Displacement (in)

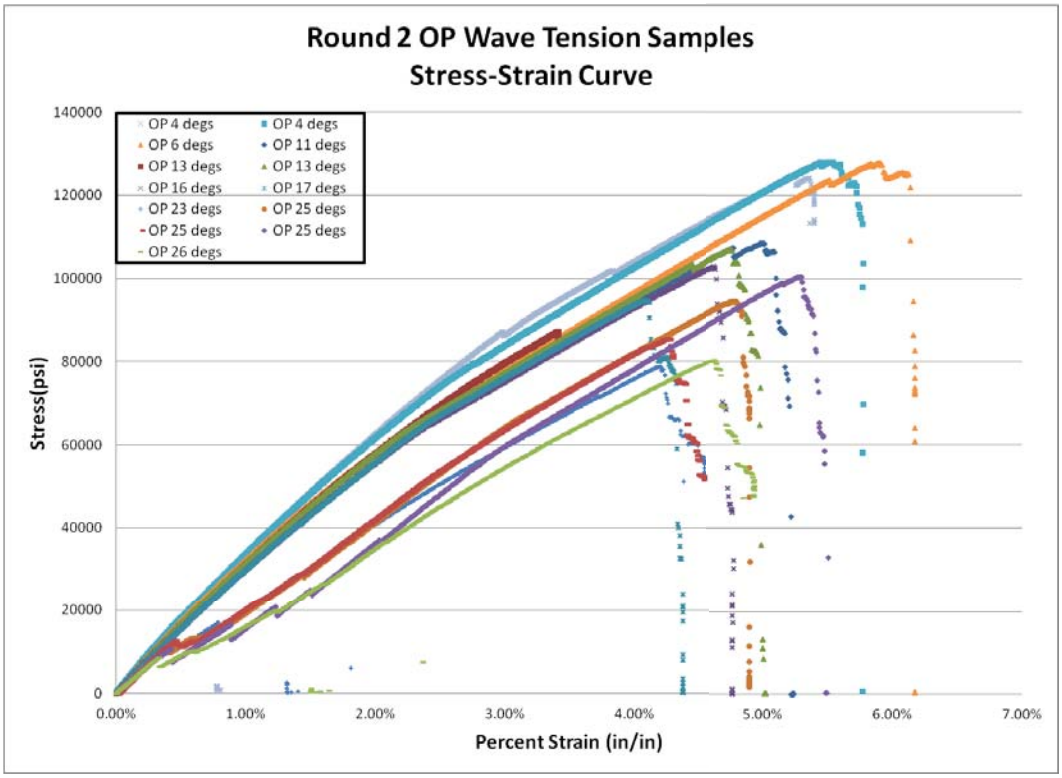
Round 2 OP Wave Tension Samples
Stress-Strain Curve
OP 4 degs
OP 4 degs
OP 6 degs
OP 11 degs
OP 13 degs
OP 13 degs
OP 16 degs
OP 17 degs
OP 23 degs
OP 25 degs
OP 25 degs
OP 25 degs
OP 26 degs
Stress(psi)
140000
120000
100000
80000
60000
40000
20000
0
0.00%
1.00%
2.00%
3.00%
4.00%
5.00%
6.00%
7.00%
Percent Strain (in/in)

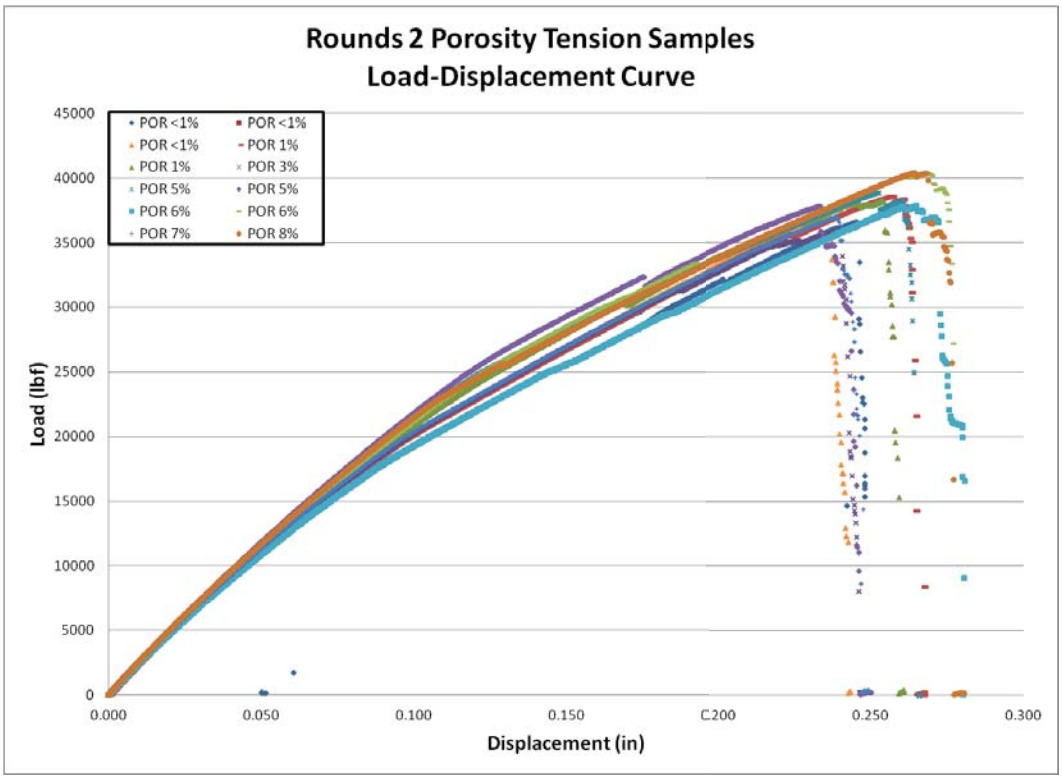
Rounds 2 Porosity Tension Samples
Load-Displacement Curve
POR <1%
POR <1%
POR <1%
POR 1%
POR 1%
POR 3%
POR 5%
POR 5%
POR 6%
POR 6%
POR 7%
POR 8%
Load (lbf)
45000
40000
35000
30000
25000
20000
15000
10000
5000
0
0.000
0.050
0.100
0.150
0.200
0.250
0.300
Displacement (in)

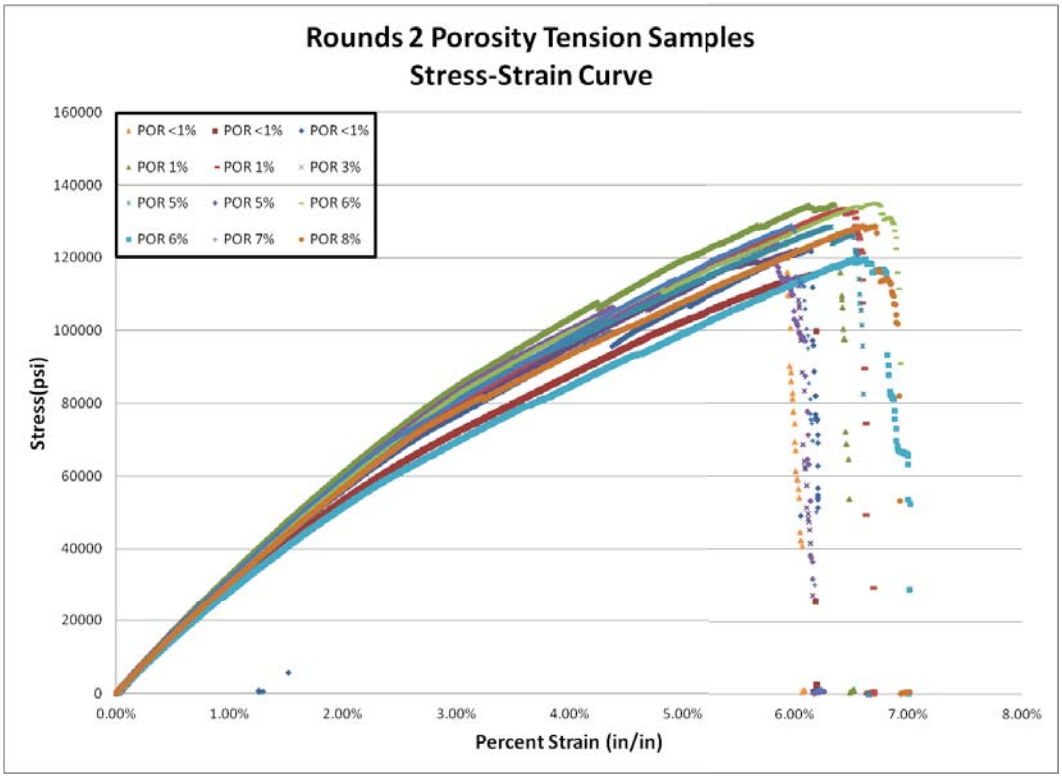
Rounds 2 Porosity Tension Samples
Stress-Strain Curve
POR <1%
POR <1%
POR <1%
POR 1%
POR 1%
POR 3%
POR 5%
POR 5%
POR 6%
POR 6%
POR 7%
POR 8%
Stress(psi)
160000
140000
120000
100000
80000
60000
40000
20000
0
0.00%
1.00%
2.00%
3.00%
4.00%
5.00%
6.00%
7.00%
8.00%
Percent Strain (in/in)

Distribution:

Emily Baca (10)
Office of Wind and Hydropower Technologies
EE-2B Forrestal Building, U.S. DOE
1000 Independence Ave. SW
Washington, DC 20585

Doug Cairns (5)
Dept. of Mechanical & Industrial Engineering
Montana State University
PO Box 173800
320 Roberts Hall
Bozeman, MT 59717-3800

Paul Veers
NREL/NWTC
1617 Cole Boulevard MS 3811
Golden, CO 80401

Scott Hughes
NREL/NWTC
1617 Cole Boulevard MS 3811
Golden, CO 80401

Derek Berry
NREL/NWTC
1617 Cole Boulevard MS 3811
Golden, CO 80401

Steve Nolet
TPI Composites Incorporated
Structural Composites Division
373 Market Street
P.O. Box 367
Warren, RI 02885-0367

Internal Distribution:

MS1124 J. Berg, 6121 (Electronic)
MS 1124 S.M. Gershin, 6122 (Electronic)
MS 1124 D.T. Griffith, 6122 (Electronic)
MS 1124 B. Hernandez-Sanchez, 6122 (Electronic)
MS 1124 D. Laird, 6122 (Electronic)
MS 1124 B. LeBlanc, 6121 (Electronic)
MS 0615 S. Neigidk 6624
MS 1124 A. Ogilvie, 6121 (Electronic)
MS 1124 J. Paquette, 6121
MS 1124 M. Rumsey, 6121 (Electronic)
MS 0615 T. Rice, 6624
MS1124 B. Resor, 6121 (Electronic)
MS 0615 D. Roach, 6620
MS1124 J. White, 6121 (Electronic)
MS 1124 Wind Library, 6121 (5)
MS 0899 Technical Library, 9536 (electronic copy)

Sandia National Laboratories